Nonlinear Negative Stiffness Wing-Tip Spring Device for Gust Loads Alleviation

A. Castrichini[1], J.E. Cooper[2]
University of Bristol, Bristol, BS8 1TH, United Kingdom

T. Wilson[3]
Airbus Operations Ltd., Filton, BS99 7AR, United Kingdom

A. Carrella[4], Y. Lemmens[5]
Siemens PLM Software, Leuven, Interleuvenlaan 68 B-3001, Belgium

A recent consideration in aircraft design is the use of folding wing-tips with the aim of having higher aspect ratio aircraft with less induced drag, but also meeting airport gate limitations. This study builds on previous work investigating the effect of exploiting folding wing-tips in-flight as a device to reduce dynamic gust loads, but now with the introduction of a passive nonlinear negative stiffness hinge spring. A single degree of freedom model and a representative civil jet aircraft aeroelastic model were used to investigate the dynamic gust response for different hinge device designs. It was found that significant reductions in the dynamic loads were possible.

Nomenclature

Symbols

b_l	=	Aerodynamic lag-pole
c	=	Mean chord
d_{cg}	=	Center of gravity/hinge line distance
D	=	Damping matrix
D_θ	=	Damping coefficient
H	=	Gust gradient
I_θ	=	Moment of inertia
F_{Aero}	=	Aerodynamic forces vector
k	=	Reduced frequency
K	=	Stiffness matrix
$K_{()}$	=	Hinge stiffness
K_o	=	Oblique spring stiffness
K_θ	=	Torsional spring stiffness
L	=	Oblique spring length
L_g	=	Gust length
m	=	Wing-tip mass
M	=	Mass matrix
$M_{()}$	=	Hinge moment
q_{dyn}	=	Dynamic pressure
q_f	=	Modal coordinates
$Q_{()}$	=	Generalized aerodynamic force matrices
Q_e	=	External forces
$Q_{i()}$	=	Coefficient matrices of RFA
Q_v	=	Quadratic velocity forces
r	=	Pulley radius
R	=	Body reference translation
R_l	=	Aerodynamic states vector
V	=	True air speed
w	=	Gust vector
w_g	=	Gust velocity
w_{g0}	=	Peak of the gust velocity
w_{ref}	=	Reference gust velocity
x_0	=	Gust origin position
x_j	=	j[th] panel's control node position
α	=	Angle of attack
γ	=	Oblique spring aspect ration
γ_j	=	j[th] panel's dihedral angle
δ	=	Aerodynamic control surfaces vector
θ	=	Wing-tip folding angle
Λ	=	Hinge orientation angle
ξ	=	Generalized coordinates vector
σ	=	Oblique spring angle
ν	=	Springs stiffness ratio
Ψ	=	Body reference rotation

Superscript

$\hat{}$	=	Nondimensional quantities
$\dot{}$	=	Differentiation with respect to time
$\tilde{}$	=	Fourier transform
$\bar{}$	=	Generalized variable

Subscript

0	=	Initial value

[1] PhD Student, Dept. of Aerospace Engineering
[2] Airbus Royal Academy of Engineering Sir George White Professor of Aerospace Engineering, AFAIAA
[3] Head of Technical Capability for Aircraft Loads Flight Physics
[4] Product Manager Test, Test Division
[5] Project Leader RTD, Aerospace Competence Centre

I. Introduction

Much effort have been made to design aircraft in order to optimize fuel consumption through reduction of aerodynamic drag. A sizable contribution to the overall drag is lift-induced drag, which could be reduced by increasing the wingspan, but such a design solution has well defined limits imposed by the maximum aircraft dimensions allowed at airports and also the increase in bending moments along the wing. A possible solution to the first issue is the use of folding wings that can be employed on the ground in a similar way to the retractable wings used on aircraft carrier borne aircraft. An example of this approach relevant to civil applications is the latest version of the B-777 which will have a folding wing capability to be activated during taxing to and from the gates. The inclusion of such a design feature raises the question as to whether such a folding device could also be used to enable loads reduction on the aircraft during the flight.

This work is aimed at studying the benefits of using a flexible wing-fold device for loads alleviation and considering how it would be implemented on civil jet aircraft. The main idea consists of introducing a hinge in order to allow the wing-tips (WT) to rotate, as shown in Fig. 1. The orientation of the hinge line relative to the direction of travel of the aircraft is a key parameter to enable successful loads alleviation[1]. When the hinge line is not along the 0° direction with respect the free stream, but is rotated outboard as in Fig. 1(b, d), folding the wing-tip then introduces a decrease in the local angle of attack. Knowing the hinge orientation Λ and the angle of rotation of the wing-tip θ the variation of the local angle of attack $\Delta\alpha_{WT}$ can be shown to be given by

$$\Delta\alpha = -\tan^{-1}(\tan\theta \sin\Lambda) \tag{1}$$

Such an effect implies that using a non $0°$ hinge angle would provide a means to reduce the loads acting on the wing. It is thus expected that moderate bend angles could lead to significant loads reductions, leading to the possibility of achieving a wing-tip extension with limited or even minimal impact on wing weight.

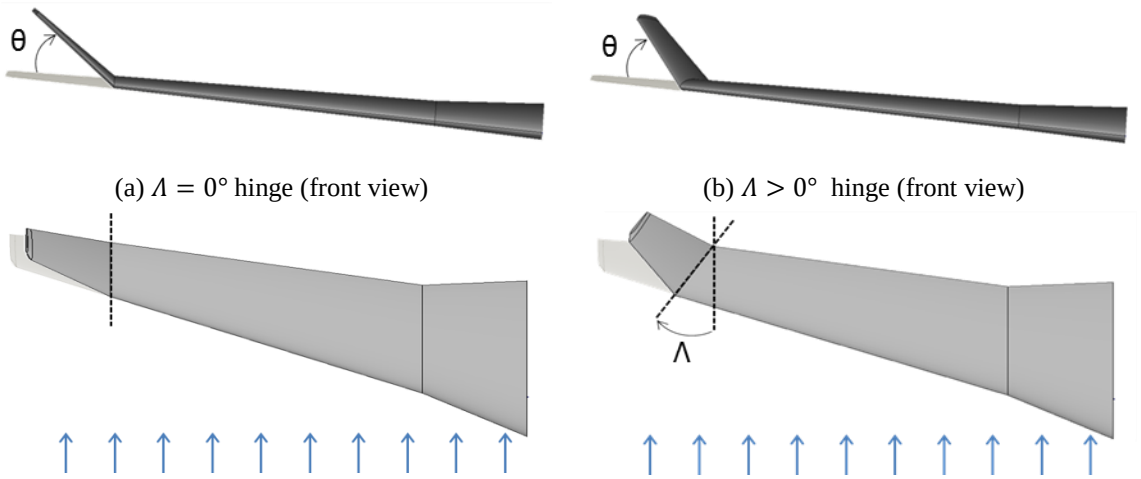

(a) $\Lambda = 0°$ hinge (front view) (b) $\Lambda > 0°$ hinge (front view)

(c) $\Lambda = 0°$ hinge (top view) (d) $\Lambda > 0°$ hinge (top view)

Figure 1. Hinge Orientations

Previous work[1] considered several structural configurations for the loads alleviation device, varying the hinge direction, wing-tip weight, linear hinge spring stiffness and linear hinge damping value for static and dynamic gust loads. Figure 2 shows the aeroelastic model used for the analyses, which was a modified version of the FFAST aeroelastic model[2] of a representative civil jet aircraft, whose structure was modelled using a "stick" model with lumped masses and the aerodynamic forces determined using the doublet lattice panel method. The main objective was to investigate the possibility of having an aircraft configuration which enables a higher aspect ratio, in order to reduce the induced drag, by limiting the increase in loads (especially in terms of wing bending moment) experienced by the aircraft, thus keeping the structure as light as possible. A baseline model, without wing-tips, Fig. 2, was considered as the reference to evaluate the benefits or the disadvantages of using the folding wing-tips, also shown in Fig. 2, which were attached to the structure using a flexible hinge, giving an increase in span of 25% compared to the baseline. Figure 3 shows a detailed view of the structural model with the attached wing-tip device.

The hinge was modeled by constraining two coincident nodes, one belonging to the main airframe and the other to the wing-tip, to have the same translations but free to have different relative rotations with respect to a predefined hinge axis.

It was shown that a quick response of the wing-tip to the gust is essential for achieving an efficient loads reduction; the phase shift between the wing root bending moment (WRBM) and the folding angle should be as small as possible to let the wing-tip alleviate the loads. Significant reductions in the resulting loads were achieved with a passive linear hinge device for small hinge stiffness, no hinge damping, reduced wing-tip weight and swept hinge. Figure 4 shows the response of a linear commercial jet aircraft model to a 83 m length gust for a baseline case and the same model but with a 25% wing-tip extension. The effect of including a 25° hinge, a linear hinge spring with $1.E0\ Nm/rad$ stiffness, no hinge damping and a $100\ Kg$ wing-tip is illustrated. Figure 4(a) shows how the model with wing-tip extensions and flexible hinges (solid line) experienced gust increment loads (in this case wing root bending moment) close to those of the model with no extensions (dotted line), whereas the extended wing with a rigid hinge suffers much larger loads (dashed line). Examination of Fig. 4(b) shows that such a good load alleviation capability was achieved thanks to a negligible phase lag between the wing-tip deflection and the increment of the wing root bending moment; such a rapid deflection allowed the wing-tip to be mostly unloaded during the gust, as shown in Fig. 4(c). The inertial loads were small due to the low weight of the device and the wing-tip rotation produced negative aerodynamic forces that balanced the upward gust contribution. The use of a higher spring stiffness, hinge damping, or wing-tip mass induced a lower and slower wing-tip deflection with a consequent worsening of the loads alleviation capability[1].

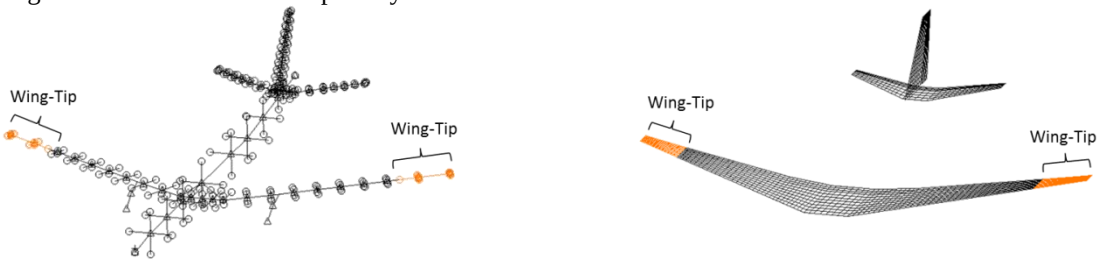

(a) Structural model (b) Aerodynamic model

Figure 2. Aeroelastic Model Showing Baseline Model and Wing-Tips

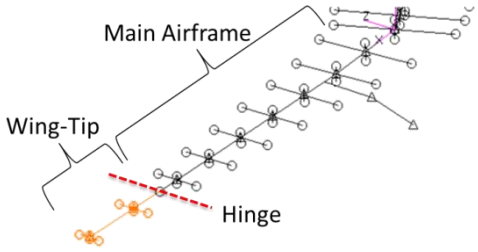

Figure 3. Folding Wing-Tip Modeling Detail

However, having such a small hinge stiffness value leads the wing-tip to be deflected during straight and level cruise flight due to the static trim loads. Such deflection is undesirable as it will be detrimental to the aerodynamic performance and trim behavior. Ideally, the wing-tip should not deflect during cruise, but only operate once a gust is encountered. With a linear hinge device there is a conflict between having a low spring stiffness for good gust loads alleviation and a high spring stiffness to counteract static trim deflections. Consequently, a compromise in the design needs to be found in order to maximize the benefits of gust alleviation whilst avoiding motion during cruise which means that sub-optimal performance is achieved.

Gatto et. al.[3] proposed the using of a composite winglet characterized by two stable configurations: under the effect of the aerodynamic loads the structure would have snapped toward a new stable configuration that generated lower aerodynamic loads, but such design did not allow to recover the original stable configuration. Furthermore the lack of a control of the "snap-through" process led to a significant dynamic loading during the passage between stable configurations. Arrieta, Bilgen et al.[4,5] addressed the problem of the implementation of the "snap-trough" process by using piezoelectric actuators in order to excite the bending resonant frequencies at the different stable

configurations of a clamped wing-tip model, resulting in a good control capability even under the effect of external aerodynamic loads.

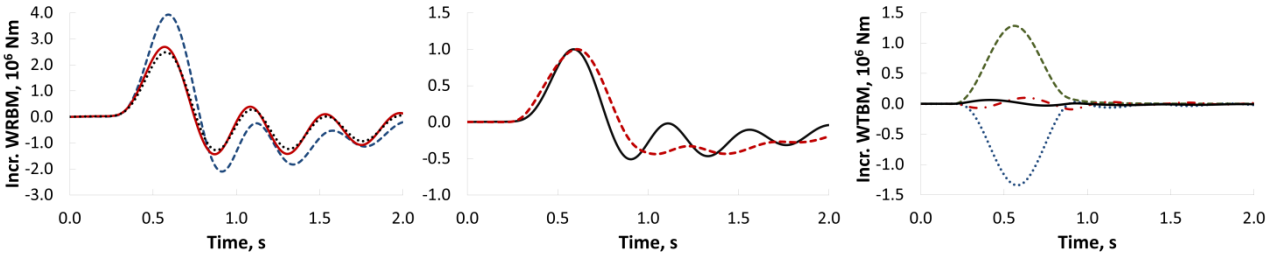

(a) Incremental WRBM comparison with the baseline and fixed hinge models (▬ ▬: fixed hinge model; ▬: flexible hinge model; ····: baseline model)

(b) Normalized incremental WRBM vs normalized incremental folding angle (▬ ▬: folding angle; ▬: WRBM)

(c) Wing-tip contribution to the Incremental WRBM (▬ ▬: gust loads; ····: aerodynamic loads due to the wing-tip deflection; ▬ · ▬: inertial loads; ▬: global loads)

Figure 4. Linear Wing-Tip Model Gust Response ($L_g = 83\ m$) ($K_\theta = 1.\ Nm/rad, D_\theta = 0.\ Nms/rad, m = 100.\ Kg$)

This paper builds upon the findings of previous work[1] that considered a linear hinge. An investigation is made into the use of a passive nonlinear hinge to the folding wing-tip concept to improve the gust loads alleviation capability. The proposed hinge device is a modified version of the high static low dynamic stiffness (HSLD) mechanism studied by Carrella et al.[6] but this time implemented for gust loads alleviation. The nonlinear spring device needs to be stiff enough to allow the wing-tip not to deflect during the cruise, whilst allowing significant rotations for significant gust events. In this way, significant wing-tip deflections are achieved when the aerodynamic loads are higher than some given threshold, allowing efficient loads alleviation.

A series of preliminary numerical simulations are performed using a single degree of freedom model and a representative civil jet aircraft aeroelastic model to investigate the influence of the design parameters on the dynamic response of the nonlinear aeroelastic systems to gusts.

II. Nonlinear Hinge Device

A. Mathematical Modeling

Nonlinear stiffness mechanisms are widely used as passive vibration isolators[6-9]. These kind of mounts are characterized by a high static low dynamic stiffness behavior: they have enough stiffness to support a given mass (high static) while having in the same time a very low natural frequency (low dynamic) which is necessary for the vibrations isolation purpose.

Several variants of nonlinear mounts have been proposed in the literature[10]; Carrella et al.[6] have provided a rigorous and analytic static investigation of a particular configuration given by a combination of a vertical spring connected in parallel with two oblique springs.

In this paper a torsional variant of the mechanism proposed by Carrella[6] was used; the nonlinear hinge device was achieved by combining a linear torsional spring, K_θ in parallel with two linear oblique springs K_o as shown in Fig. 5. Furthermore, a pulley was introduced to convert the axial forces provided by the oblique springs into a torque applied on the hinge line.

When only the oblique springs are employed, the resulting moment on the wing-tip hinge is given by

$$M_{nl} = 2K_o r(L_0 - L)\sin\sigma \tag{2}$$

where L is the actual length of the oblique springs, σ is the angle of inclination of the oblique springs, K_o is the related linear stiffness and r is the radius of the pulley. By consideration of the geometry, $\sin\sigma = \frac{h_0 - r\theta}{L}$; $L = \sqrt{(h_0 - r(\theta - \theta_0))^2 + a^2}$; $L_0 = \sqrt{h_0^2 + a^2}$ and the non-dimensional parameters $\gamma = \frac{a}{L_0} = \cos\sigma_0$ and $\hat{r} = \frac{r}{L_0}$; the nonlinear moment given by the oblique springs can be expressed as

$$M_{nl} = K_o r^2 \widehat{M}_{nl}$$
$$= K_o r^2 \frac{2}{\hat{r}}\left(\sqrt{1-\gamma^2} - \hat{r}(\theta-\theta_0)\right)\left[\left(\hat{r}^2(\theta-\theta_0)^2 - 2\sqrt{1-\gamma^2}\hat{r}(\theta-\theta_0)+1\right)^{-1/2} - 1\right] \quad (3)$$

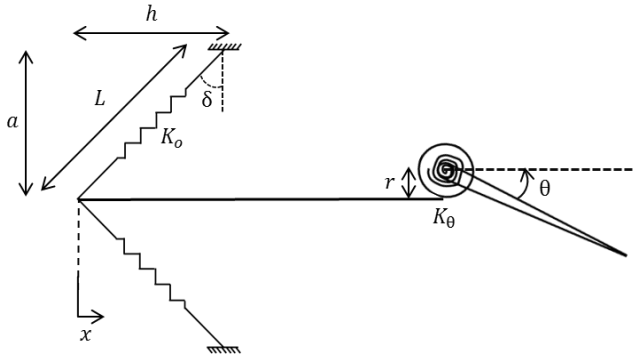

Figure 5. Schematic Representation of the Nonlinear Spring Device

The non-dimensional parameters γ and $\hat{r}$ define the geometry of the nonlinear device. γ represents the aspect ratio of the oblique springs and for $\gamma = 0$ the springs are initially horizontal while for $\gamma = 1$ the springs are initially vertical. $\hat{r}$ represents the aspect ratio of the pulley with respect the oblique springs initial length, the higher that $\hat{r}$ is the greater the longitudinal displacement of the oblique springs x for a given wing-tip rotation. Such a configuration is characterized by three equilibrium points when $\widehat{M}_{nl}(\theta) = 0$, given by

$$\theta_1^{eq} = \theta_0; \qquad \theta_2^{eq} = \frac{\sqrt{1-\gamma^2}}{\hat{r}} + \theta_0; \qquad \theta_3^{eq} = 2\frac{\sqrt{1-\gamma^2}}{\hat{r}} + \theta_0 \quad (4)$$

and, as expected, θ_1^{eq} and θ_3^{eq} are symmetric with respect θ_2^{eq} due to the symmetry of the nonlinear device.

The related non-dimensional stiffness is evaluated by deriving $\widehat{M}_{nl}$ with respect to the angle of rotation θ as

$$\widehat{K}_{nl} = \frac{d\widehat{M}_{nl}}{d\theta} = 2\left[1 - \gamma^2\left(\hat{r}^2(\theta-\theta_0)^2 - 2\sqrt{1-\gamma^2}\hat{r}(\theta-\theta_0)+1\right)^{-3/2}\right] \quad (5)$$

The stiffness $\widehat{K}_{nl}$ is zero when

$$\theta_{1,2}^{stab} = \theta_2^{eq} \pm \frac{\sqrt{\gamma^{4/3} - \gamma^2}}{\hat{r}} \quad (6)$$

which define the stability boundaries of the nonlinear springs. The interval $(\theta_1^{stab};\ \theta_2^{stab})$ represents the unstable branch of the nonlinear moment curve $\widehat{M}_{nl}(\theta)$ where $\widehat{K}_{nl}$ is negative, i.e. the springs would provide a hinge moment in the folding angle direction.

When $\gamma = 1$ there is only one equilibrium point and $\theta_{1,2,3}^{eq} = \theta_{1,2}^{stab} = \theta_0$, for $\gamma < 1$ all the points are distinct and $\theta_1^{eq} < \theta_1^{stab} < \theta_2^{eq} < \theta_2^{stab} < \theta_3^{eq}$; therefore θ_1^{eq} and θ_3^{eq} are stable equilibrium points being characterized by a positive stiffness value, while θ_2^{eq} is unstable being $\widehat{K}_{nl}\left(\theta_2^{eq}\right) < 0$. In the specific case θ_2^{eq} represents the configuration when the oblique springs are vertical.

When a linear torsional spring K_θ is put in parallel with the oblique springs, the overall structural moment and stiffness are given by

$$M_{struct} = K_\theta \widehat{M}_{struct} = K_\theta\left[(\theta-\theta_0) + \nu\widehat{M}_{nl}\right] = K_\theta\left(\widehat{M}_l + \nu\widehat{M}_{nl}\right) \quad (7)$$

$$K_{struct} = K_\theta \frac{d\widehat{M}_{struct}}{d\theta} = K_\theta\left(1 + \nu\widehat{K}_{nl}\right) \tag{8}$$

where $\nu = \frac{K_o r^2}{K_\theta}$ is the ratio of the equivalent torsional stiffness of the oblique springs, $K_o r^2$, with the linear torsional spring K_θ.

Figure 6 shows the effects on the non-dimensional structural hinge moment $\widehat{M}_{struct}$ and stiffness $\widehat{K}_{struct}$ of the design parameter $\gamma,\ \hat{r}, \nu$. The characteristic "S" shape of the nonlinear moment curve is due to the nonlinearity introduced by the oblique springs, for $\theta_1^{stab} < \theta < \theta_2^{stab}$ these provide a negative stiffness contribution that can overcome the positive stiffness of the linear spring for a given interval of rotations θ. This nonlinear effect is more or less pronounced as a function of the geometry of the system $\gamma,\ \hat{r}$ and the stiffness ratio value ν. For $\gamma = 0$ the springs are initially horizontal, while they are initially vertical for $\gamma = 1$. The lower that γ is, the more the oblique springs absorb potential energy during the wing-tip rotation and so the greater the nonlinear "snap through" mechanism of the oblique springs becomes dominant. The higher that $\hat{r}$ is, the smaller the interval $\Delta\theta$ in which the oblique springs provides a negative stiffness contribution being $\theta_{1,2}^{stab} \propto \hat{r}^{-1}$. The higher that the stiffness ratio is, the higher the contribution of the oblique springs over the linear torsional one, but since it does not affect $\theta_{1,2}^{stab}$, as showed in Eq. (6), the range of rotation over which the oblique springs provide a negative stiffness contribution does not change with ν.

When the oblique springs are combined with a linear torsional spring, it is not possible anymore to have a closed form formulation of the equilibrium points of the system as a function of the design parameters. A bifurcation analysis was performed to investigate the dependency of the number of the equilibrium points with $\gamma,\ \hat{r}, \nu$. Figure 7 shows the bifurcation diagram of the mechanical system and it has been found that the number of the equilibrium points was solely a function of the $\gamma - \nu$ combination, while $\hat{r}$ did not have any effect. The system exhibited a bistable behavior in the grey region in Fig. 7, being characterized by three equilibrium points (2 stable and 1 unstable), while the white region allowed only one stable equilibrium point.

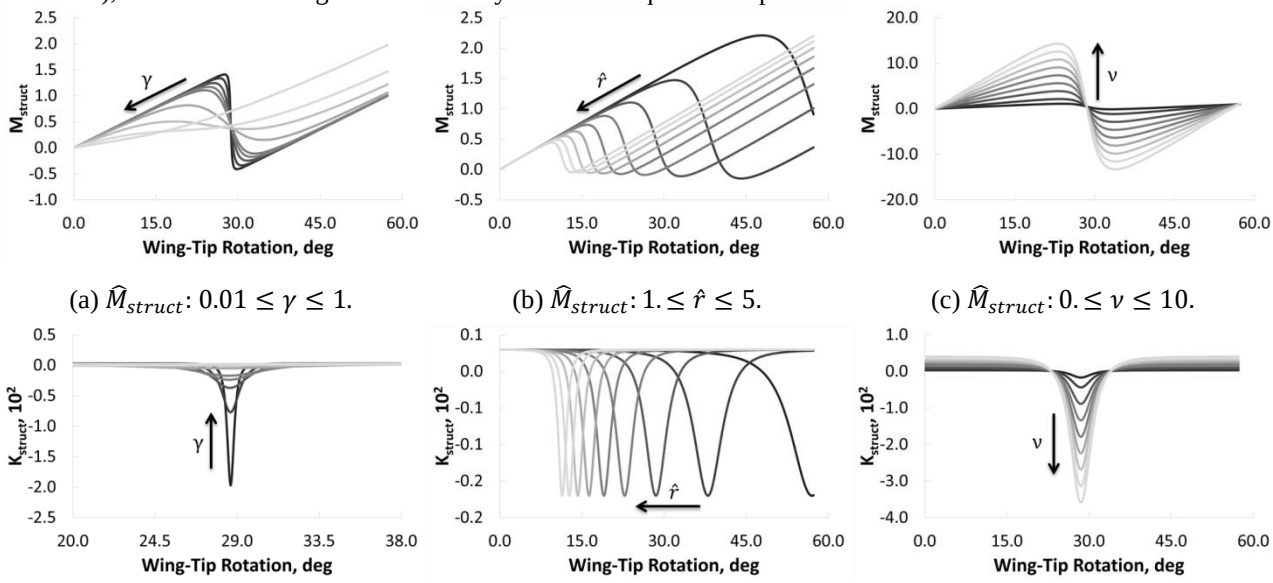

(a) $\widehat{M}_{struct}$: $0.01 \le \gamma \le 1.$ (b) $\widehat{M}_{struct}$: $1. \le \hat{r} \le 5.$ (c) $\widehat{M}_{struct}$: $0. \le \nu \le 10.$

(d) $\widehat{K}_{struct}$: $0.01 \le \gamma \le 1.$ (e) $\widehat{K}_{struct}$: $\hat{r} = 1. \le \hat{r} \le 5.$ (f) $\widehat{K}_{struct}$: $\nu = 0. \le \nu \le 10.$

Figure 6. Nonlinear Moment and Stiffness Curves

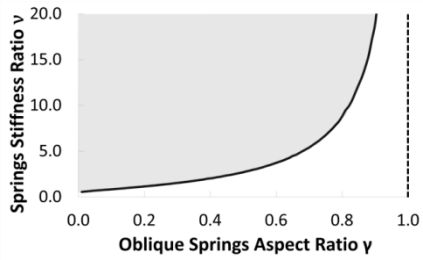

Figure 7. Bifurcation Diagram (grey region: 3 equilibrium points; white region: 1 equilibrium point)

B. High Static Low Dynamic Aeroelastic Stiffness Design

When the overall aeroelastic system is considered, the hinge device stiffness is characterized not only by the positive stiffness provided by the linear torsional spring and the negative stiffness, for $\theta_1^{stab} < \theta < \theta_2^{stab}$, of the oblique springs, but also by a positive stiffness contribution due to the aerodynamic forces for $\Lambda > 0$. For an outboard rotated hinge sweep angle, an upward wing-tip deflection produces a decrease in the local angle of attack leading to the generation of incremental aerodynamic forces that oppose the wing-tip deflection.

The concept behind a high static and low dynamic aeroelastic stiffness hinge mechanism is to design a spring that is stiff enough to keep the wing-tip trimmed during cruise, but then to take advantage of the negative stiffness regime provided by the oblique springs in order to allow a rapid rotation of the folding wing-tip during a gust event and so achieve an efficient reduction of the related gust loads without degrading the aerodynamic trim performance; the device should be able as well to return to an undeflected configuration after the gust event. Figure 8 shows the schematic operation of the device. The wing-tip is attached to the springs with an initial downwards deflection angle when no aerodynamic forces are applied. At the trim flight configuration, the aerodynamic forces generate a rotation of the wing-tip, the oblique springs would be then be compressed to assume a vertical configuration and the static load would be taken mainly by the linear torsional spring. In such a configuration, the oblique springs would not generate any moment, but they would provide a negative stiffness contribution that, counteracting the positive structural and aerodynamic moments, would allow a rapid deflection of the wing-tip in the case of a gust event. The negative aerodynamic forces generated by the upward rotation would lead the system to move to the original position.

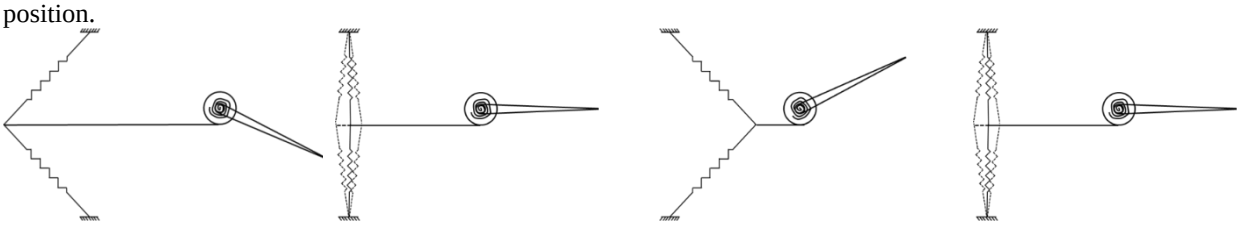

(a) Initial deflection (b) Trim configuration (c) Gust deflection (d) Trim configuration

Figure 8. Schematic of Wing-Tip Operation

The overall static aeroelastic hinge moment and stiffness can be expressed as

$$M_{tot} = M_{struct} - K_{aero\theta}\theta - M_{ext} \tag{9}$$

$$K_{tot} = K_{struct} - K_{aero\theta} \tag{10}$$

where M_{struct} and K_{struct} are the structural moment and stiffness given by the linear and nonlinear springs combination as in Eqs. (7) and (8); $K_{aero\theta}$ is the wing-tip aerodynamic stiffness that defines the hinge moment contribution due to the aerodynamic forces generated by the wing-tip deflection; the latter represents the overall hinge moment due to the combination of the external static loads, such the aerodynamic trim loads or the gravitational loads.

In order to let the hinge device behave with a high static low dynamic aeroelastic spring stiffness, it was required that the wing-tip was undeflected at the horizontal trimmed flight condition. Assuming as known the overall static

external moments acting on the hinge, and assuming that no oblique springs are employed, the value of the linear spring stiffness that satisfies the $\theta_{trim} = 0°$ condition is given by

$$K_\theta = \frac{M_{ext}}{\theta_0} \tag{11}$$

When oblique springs are also considered, to let the nonlinear device to have the same static equilibrium point as the linear device for the same flight condition, it is required that the oblique springs do not provide any moment, which infers $\theta_2^{eq} = \theta_{trim} = 0°$. From Eq. (4), this condition leads to the definition of the non-dimensional radius as

$$\hat{r} = \frac{\sqrt{1-\gamma^2}}{\theta_0} \tag{12}$$

for given values of θ_0 and γ. When Eq. (12) is satisfied the equilibrium point of the nonlinear system does not change by varying the stiffness of the oblique springs, since in Eq. (4) it has been shown that θ_2^{eq} (and so θ_{trim}) is not a function of ν. Therefore the oblique springs stiffness can be used as a tuning parameter to calibrate the overall stiffness of the hinge device around the equilibrium point. An interesting value for ν can be found when Eq. (10) is evaluated at $\theta_{trim} = 0°$ and set to zero to achieve a "quasi-zero-aeroelastic-stiffness" at the equilibrium point. The spring stiffness ratio to achieve this is given by

$$\nu_{qzas} = \frac{\gamma(1+\nu_{aero})}{2(1-\gamma)} \tag{13}$$

where $\nu_{aero} = \frac{K_{aero\theta}}{K_\theta}$ is the ratio of the torsional aerodynamic stiffness, $K_{aero\theta}$, to the linear torsional spring K_θ.

A value of $\nu < \nu_{qzas}$ would allow the system to have only one stable equilibrium point, while $\nu > \nu_{qzas}$ would lead to three possible equilibrium points of which $\theta_{trim} = 0°$ is unstable due to the negative aeroelastic stiffness K_{tot}. If Eq. (8) is evaluated at $\theta_{trim} = 0°$ and set to zero the value of the spring stiffness ratio that leads to a "quasi-zero-structural-stiffness"[6] is given by

$$\nu_{qzss} = \frac{\gamma}{2(1-\gamma)} \tag{14}$$

When Eqs.(11) and (12) are satisfied and $\nu_{qzss} \leq \nu \leq \nu_{qzas}$, the hinge device behaves as a high static low dynamic aeroelastic stiffness device exhibiting only one equilibrium point, a negative structural stiffness and a positive aeroelastic stiffness. Figure 9 shows the typical $M_{tot}(\theta)$ trend for a high static low dynamic aeroelastic stiffness design.

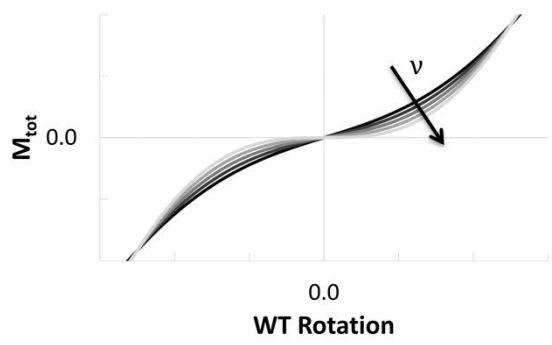

Figure 9. High Static Low Dynamic Stiffness Spring Design – Aeroelastic Moment vs Folding Angle

III. Single Degree of Freedom Model

The high static low dynamic aeroelastic stiffness hinge device, introduced in the previous section, is applied here to a single degree of freedom model. The aim of such investigation was to achieve a good understanding of the isolated dynamic response of such device when no structural dynamic coupling with the main airframe is considered.

A. Structural Modelling

Figure 10(a) shows the structural model that was be used for the analyses, which is given by a rigid stick structural model with lumped masses. The wing-tip preserves the same geometry and mass distribution of the $100\ Kg$ folding devices considered previously[1]. The structural model has only one degree of freedom given by the rigid rotation around a hinge axis at the wing-tip's root. The nonlinear torsional spring was defined on the hinge.

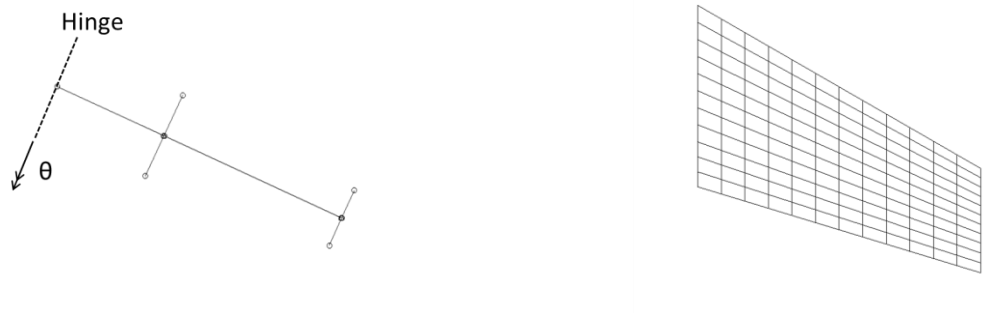

(a) Structural model (b) Aerodynamic model

Figure10. SDOF Wing-Tip Aeroelastic Model (top view)

B. Aerodynamic Modelling

The wing-tip aerodynamic mesh is showed in Fig. 10(b), where the doublet lattice method[11,12] was employed to model the hinge moment due to the aerodynamic forces which, in the frequency domain, is defined as

$$M_{aero} = q_{dyn}[Q\tilde{\theta} + Q_g\tilde{w}] \tag{15}$$

where $Q_{(1\ X\ 1)}$ and $Q_{g(1\ X\ N_{Panels})}$ are the generalized aerodynamic forces matrices related to the Fourier transform of the generalized coordinate $\tilde{\theta}$ and the gust vector $\tilde{w}$. The latter defines the downwash on a generic aerodynamic panel *j* due to the gust such that

$$w_j = \cos\gamma_j \frac{w_{g0}}{2V}\left(1 - \cos\left(\frac{2\pi V}{L_g}\left(t - \frac{x_0 - x_j}{V}\right)\right)\right) \tag{16}$$

where L_g is the gust length (twice the gust gradient *H*), V is the true air speed and w_{g0} peak gust velocity. The latter defined (in m) as[13]

$$w_{g0} = w_{ref}\left(\frac{H}{106.17}\right)^{\frac{1}{6}} \tag{17}$$

In order to allow for simulation in the time domain, the aerodynamic matrices were approximated, in the frequency domain, using the rational fraction approximation method proposed by Roger[14]. Following some manipulation and taking into account also of the static aerodynamic forces due to a prescribed trim angle of attack α, the aerodynamic loads can be formulated in the time domain as

$$M_{aero} = q_{dyn}\left\{\left[Q_0(\theta-\theta_{\alpha_{0L}}) + \frac{c}{2V}Q_1\dot{\theta} + \left(\frac{c}{2V}\right)^2 Q_2\ddot{\theta}\right] + \left[Q_{g0}w + \frac{c}{2V}Q_{g1}\dot{w} + \left(\frac{c}{2V}\right)^2 Q_{g2}\ddot{w}\right] + \sum_{l=1}^{N_{Poles}} R_l + Q_{\alpha 0}(\alpha-\alpha_{0L})\right\} \tag{18}$$

where R_l is the generic aerodynamic state vector related to the generic lag-pole $\left(b_l = \frac{k_{max}}{l}\right)$. These extra states allow modeling of the unsteady response of the aerodynamics by taking into account the delay of the aerodynamic forces with respect to the structural deformations. These aerodynamic states were evaluated through the set of dynamic equations

$$\dot{R}_l = -b_l\frac{2V}{c}IR_l + Q_{2+l}\dot{\theta} + Q_{g2+l}\dot{w} \qquad l = 1,\dots,N_{Poles} \tag{19}$$

For this paper it was assumed a zero zero-lift angle of attack $\alpha_{0L} = 0$, a non zero value could be defined to take into account the effect of the camber of the wing-tip's aerodynamic airfoils on the related $C_L(\alpha)$ curve. From Eq. (1), the $\alpha = \alpha_{0L}$ condition is given for an angle of rotation of $\theta = \theta_{\alpha_{0L}} = -\tan^{-1}\left(\frac{\tan\alpha_{0L}}{\sin\Lambda}\right)$.

The generic aerodynamic matrices Q and Q_g are a strict function of the hinge angle Λ and Fig. 11 shows the trend of the aerodynamic stiffness terms Q_0 and $Q_{\alpha 0}$. Figure 12(a) shows that when the hinge is inboard rotated ($\Lambda < 0$) the aerodynamic stiffness Q_0 is positive, leading to positive aerodynamic forces for an upward rotation of the wing-tip, as seen in Fig. 12(b). Such a design leads to a statically unstable system and will also reduce the loads alleviation capability; following a gust event the wing-tip would have a positive rotation and the generated upward aerodynamic forces would give a further increase of the overall loads. For these reasons only outboard rotated hinges may allow loads alleviation. A value of $\Lambda = 25°$ was considered for this work.

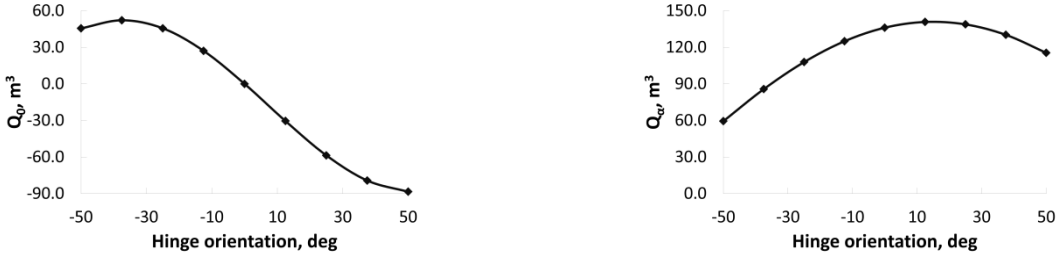

(a) $Q_0(\Lambda)$. (b) $Q_{\alpha 0}(\Lambda)$.

Figure 11. Aerodynamic Stiffness vs Hinge Orientation

(a) $\Lambda > 0$. (b) $\Lambda < 0$.

Figure 12. Aerodynamic Forces Distribution for an Upward Wing-Tip Rotation ($\theta > 0$.)

C. Equation of Motion

The nonlinear dynamic equation of the system is described as

$$I_\theta \ddot{\theta} + D_\theta \dot{\theta} + K_\theta(\theta - \theta_0) + M_{nl} = M_{aero} + mgd_{CG}\cos\theta \tag{20}$$

where θ_0 is the initial wing-tip deflection, I_θ is the moment of inertia of the structure, D_θ is the hinge damping coefficient, K_θ is the linear hinge spring stiffness, M_{nl} is the nonlinear moment provided by the oblique springs, M_{aero} is the aerodynamic moment and $mgd_{CG}\cos\theta$ represents the moment due to the gravity, where d_{CG} is the distance of the center of gravity from the hinge. Both d_{CG} and I_θ are functions of the hinge orientation Λ and the mass distribution of the folding device. This paper focuses on the structural design of the nonlinear hinge spring, so the effect of the mass and the hinge orientation, already discussed in a previous work[1], were not investigated. For all the presented results it is assumed that $m = 100\ Kg$ and $\Lambda = 25°$.

Recasting Eq. (9) for the single degree of freedom model leads to the following formulation for the overall static aeroelastic hinge moment such that

$$M_{tot} = M_{struct} - q_{dyn}Q_0\left(\theta - \theta_{\alpha_{0L}}\right) - q_{dyn}Q_{\alpha 0}(\alpha - \alpha_{0L}) - mgd_{CG}\cos\theta \tag{21}$$

whose related aeroelastic stiffness is given by

$$K_{tot} = K_{struct} - q_{dyn}Q_0 + mgd_{CG}\sin\theta \tag{22}$$

where $q_{dyn}Q_0$ represents the aerodynamic stiffness $K_{aero\theta}$ of Eqs. (9) and (10).

Equation (21) highlights how the static aeroelastic hinge moment is not only a function of the structural design parameters but also of the flight condition. In particular, the term $q_{dyn}Q_{\alpha 0}(\alpha - \alpha_{0L})$ represents the static load contribution due to the dynamic pressure and the angle of attack that can affect the number of equilibrium points of the system for a given structural design. The equilibrium points of the complete aeroelastic system are given by the roots of the static aeroelastic hinge moment reported in Eq. (21). Figure 13 shows the qualitative evolution of M_{tot} for two different generic structural designs by keeping the dynamic pressure fixed and varying the angle of attack α: $0° \rightarrow 8°$. The general effect is a shift in the downwards direction of the moment curve with the increment of α, this could lead the system to pass from having only one equilibrium point to three equilibrium points, as showed in Fig. 13(b). This kind of bifurcation may arise only for those structural designs and dynamic pressures that allow negative aeroelastic stiffness K_{tot} for a range of rotation angles θ.

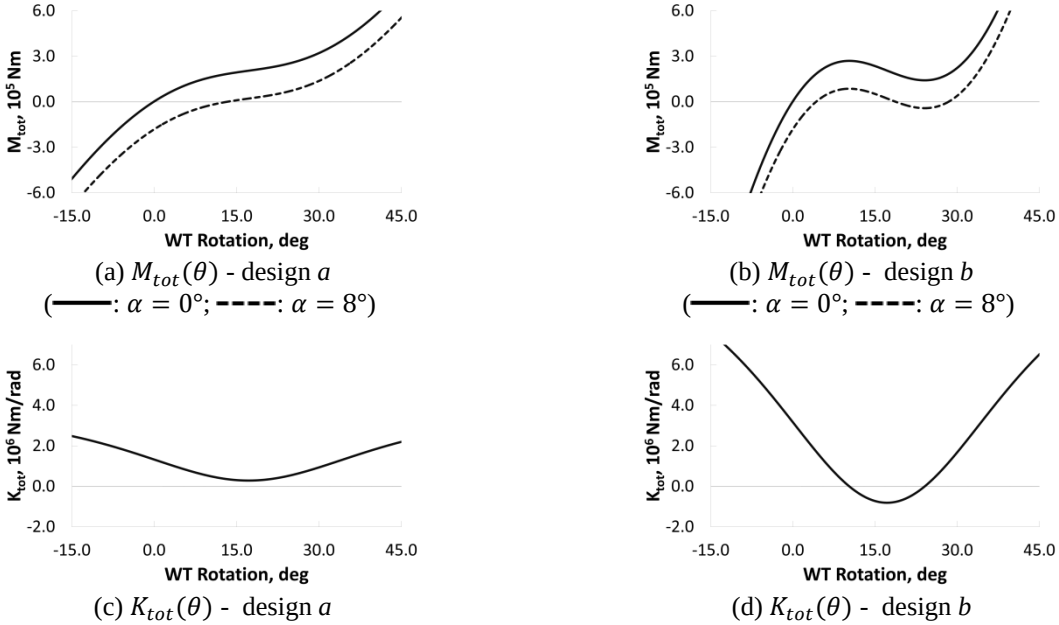

(a) $M_{tot}(\theta)$ - design *a* (——: $\alpha = 0°$; - - - -: $\alpha = 8°$)

(b) $M_{tot}(\theta)$ - design *b* (——: $\alpha = 0°$; - - - -: $\alpha = 8°$)

(c) $K_{tot}(\theta)$ - design *a*

(d) $K_{tot}(\theta)$ - design *b*

Figure 13. Effect of α on the System's Equilibrium Points

D. Results

Several aeroelastic analyses were performed to investigate the dynamic response of the folding wing-tip for different structural designs.

Being the structural model nonlinear, it was no possible to evaluate separately the static and dynamics responses and then superimpose the single effects, therefore the dynamic gust response analyses were performed starting from the trimmed flight configuration. A "1-g" load case was considered with the wing-tip operating at $M = 0.6$ at $25{,}000\ ft$, equivalent to a dynamic pressure of $9.47\ KPa$ and at an angle of attack of $\alpha = 6.25°$. Several aeroelastic analyses were then made over a range of gust lengths. With reference to Eq. (17), w_{ref} was varied linearly from $13.4\ m/s$ EAS at $15{,}000\ ft$ to $7.9\ m/s$ EAS at $50{,}000\ ft$, based on the FAA Federal Aviation Regulations. At the investigated flight altitude of $25{,}000\ ft$ and Mach number of $M = 0.6$, the gust reference velocity was $11.48\ m/s$ EAS, while the gust lengths varied between $18\ m$ and $214\ m$.

1. Linear Hinge Model

It has been demonstrated[1] that when a linear hinge spring was used, an effective loads alleviation was possible only when the response of wing-tip was rapid enough to produce downwards aerodynamic forces that balanced the upward gust loads contribution so that the wing-tip was almost unloaded during the gust event. In terms of structural characteristics this means that an outboard rotated hinge, low wing-tip mass, no damping and negligible spring stiffness were used.

Since a single degree of freedom model was considered, the hinge moment was the only load information that could be retrieved. As the loads were given mainly by the balance of gust, aerodynamic and inertial vertical forces acting on the wing-tip, it was assumed that the trend of the global hinge moment would reflect qualitatively the contribution of the wing-tip on the wing root bending moment when a full aircraft model was considered.

Figures 14 and 15 show maximum incremental loads and the wing-tip deflections due to a family of "1-cosine" gusts for four structural configurations with the same mass $m = 100\ Kg$, hinge direction $\Lambda = 25.°$, no hinge damping element, but different initial deflections and spring stiffness: $[\theta_0 = 0.°;\ K_\theta \approx \infty\ Nm/rad]$, $[\theta_0 = 0.°;\ K_\theta = 0.\ Nm/rad]$, $[\theta_0 = -12.5°;\ K_\theta = 6.434E05\ Nm/rad]$ and $[\theta_0 = -25.°; K_\theta = 3.217E05\ Nm/rad]$. The stiffness of the two latter configurations was defined according to Eq. (11). As expected the maximum loads were experienced by the fixed hinge model while, for the other configurations, the lower the hinge stiffness, the lower the resulting loads. In particular, it was found that setting $K_\theta \approx 0.\ Nm/rad$ provided the best loads alleviation leading to gusts that did not provide any further increment to the hinge moment, the drawback was the significant wing-tip deflection due to the static aerodynamic trim loads, Fig. 15(a), and so a consequent worsening of the trim aerodynamic performance. An intermediate solution can be found by employing a spring stiffness as defined by Eq. (11) for a given θ_0 and flight condition.

Figure 16 shows the time histories of the hinge moment for the same structural configurations and a fixed gust length of $L_g = 104.m$. It is demonstrated how very low spring stiffness $K_\theta \approx 0.\ Nm/rad$ allows the wing-tip to deflect enough to generate negative lift to balance the positive gust contribution; a higher spring stiffness leads to a lower deflection resulting in a worse loads alleviation performance.

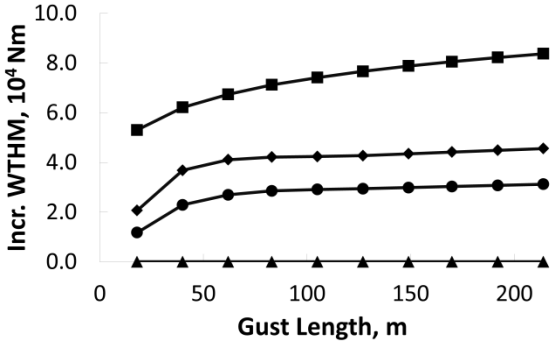

Figure 14. Linear Gust Response - Maximum Incremental Wing-Tip Hinge Moments vs Gust Lengths (■: $K_\theta \approx \infty\ Nm/rad$; ▲: $K_\theta \approx 0.\ Nm/rad$; ●: $K_\theta = 3.217E05\ Nm/rad$; ◆: $K_\theta = 6.434E05\ Nm/rad$)

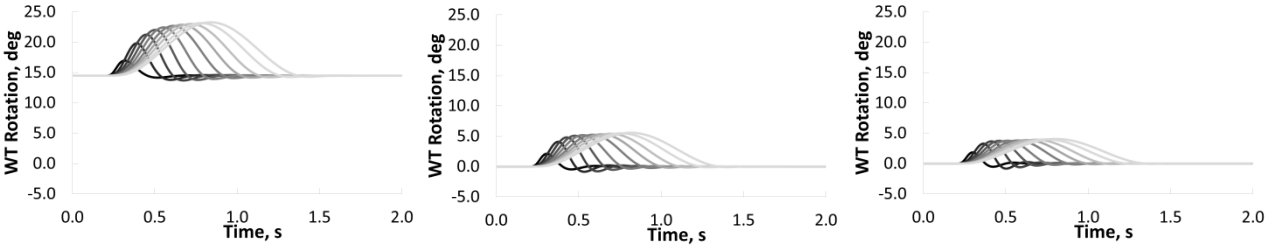

(a) $K_\theta \approx 0. Nm/rad$ (b) $K_\theta = 3.217E05\ Nm/rad$ (b) $K_\theta = 6.434E05\ Nm/rad$

Figure 15. Linear Gust Response - Wing-tip Deflection vs Time

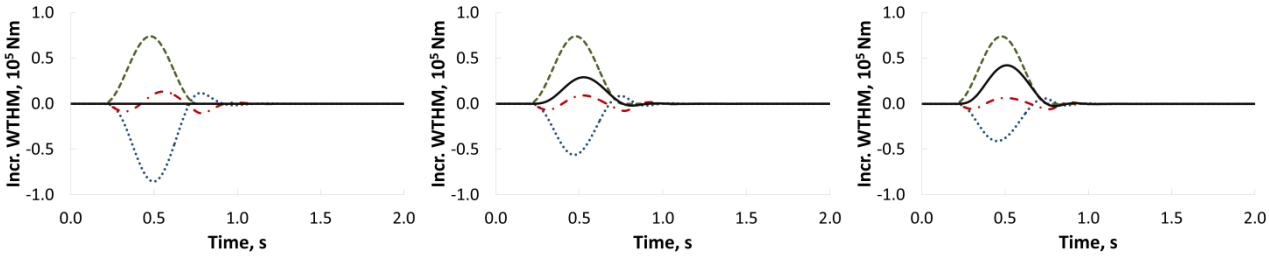

(a) $K_\theta \approx 0. Nm/rad$ (b) $K_\theta = 3.217E05\ Nm/rad$ (b) $K_\theta = 6.434E05\ Nm/rad$

Figure 16. Incremental Unsteady Gust Loads vs Time for $L_g = 104.m$
(– – –: gust loads; ·····: aerodynamic loads due to the wing-tip deflection; – · –: inertial loads; ——: global loads)

2. Nonlinear Hinge Model

Several structural configurations were considered, varying the hinge device design parameters according the high static low dynamic aeroelastic stiffness concept introduced in the previous section. Four different spring designs have been considered for the nonlinear gust response analyses: upon the linear models of the previous section $[\theta_0 = -25.°;\ K_\theta = 3.217E05\ Nm/rad]$ and $[\theta_0 = -12.5.°;\ K_\theta = 6.434E05\ Nm/rad]$, were defined two sets of oblique springs with an inclination of $\sigma_0 = 30.°$ ($\gamma = 0.866$) and $\sigma_0 = 60.°$ ($\gamma = 0.5$). The related adimensional pulley radii $\hat{r}$ were defined according Eq. (12). For each of the four configurations the spring stiffness ratio ν was then varied between the values ν_{qzas} and ν_{qzss}.

Figure 17 shows the loads envelope for different gust lengths and the overall moment and stiffness for the $[\theta_0 = -25.°;\ K_\theta = 3.217E05\ Nm/rad\ ; \gamma = 0.866;\ \hat{r} = 1.15]$ configuration for different values of the spring stiffness ratio ν. The higher that ν was, the lower the stiffness of the system at the equilibrium point and so the better the loads alleviation performance. In particular the loads were always lower than those of the linear model with $K_\theta = 3.217E05\ Nm/rad$. Furthermore for such a configuration $\nu_{qzss} = 3.23$ and $\nu_{qzas} = 8.81$, so it can be seen that when $\nu = \nu_{qzss}$ the overall aeroelastic stiffness of the nonlinear model was locally equal to that of the linear system when $K_\theta \approx 0. Nm/rad$ (dotted line Fig. 17(c)) around the equilibrium point, leading the wing-tip to experience an almost zero incremental hinge moment during a gust event. When $\nu_{qzss} < \nu < \nu_{qzas}$ the aeroelastic stiffness of the system was even lower than that of the linear system with $K_\theta \approx 0. Nm/rad$, allowing negative values of the maximum hinge moment despite the positive gust loads.

A better understanding of the system response can be found by looking at the time histories of the loads for this configuration, for a given gust lengths, $L_g = 104.m$, and for different values of ν, as shown in Fig. 18. For $\nu = 3.23$ the folding device generated just enough negative lift variation to balance the positive gust increment; when $\nu = 6.02$, the lower aeroelastic stiffness allowed higher wing-tip rotations and so the generation of negative aerodynamic forces that overcame the positive gust loads and this trend was even more emphasized for $\nu = 8.81$. The drawback in using a higher value of ν was that the folding device needed a longer time to recover the undeflected trim configuration because of the very low stiffness value, as demonstrated by the slower decay of the negative lift contribution due to the wing-tip deflection showed in Fig. 18(c) (dotted line).

Figure 19 shows a comparison between the displacements of the linear and nonlinear models sharing the same linear torsional spring, demonstrating that the nonlinear springs enable higher rotations and so a better loads alleviation with respect to the linear model, whilst still allowing the system to recover the original undeflected configuration after the gust event.

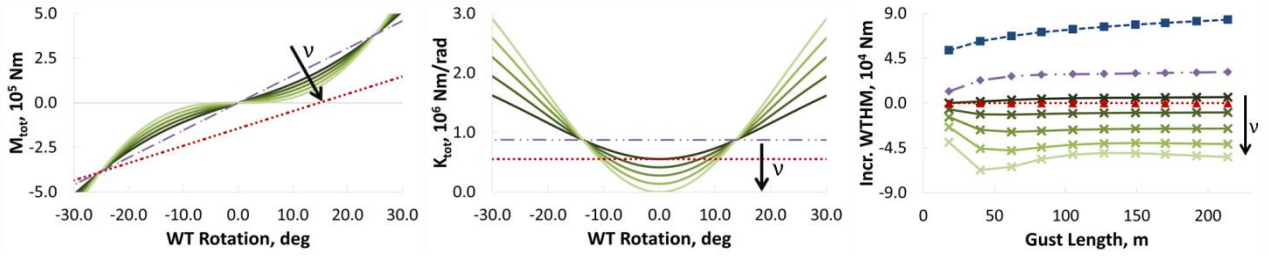

(a) $M_{tot}(\theta)$ (b) $K_{tot}(\theta)$ (c) Loads Envelope vs Gust Lengths

Figure 17. Nonlinear Gust Response
$\theta_0 = -25.°$; $K_\theta = 3.217E05\, Nm/rad$; $\gamma = 0.866$; $\hat{r} = 1.15$; $\nu = [3.23, 4.63, 6.02, 7.42, 8.81]$
(- - - -: fixed hinge model; — · · —: linear model $K_\theta = 3.217E05\, Nm/rad$;
·····: linear model $K_\theta = 0.\, Nm/rad$; ——: nonlinear model)

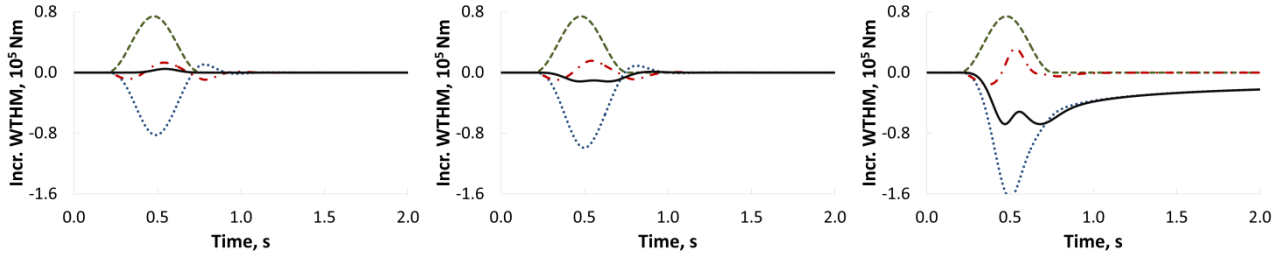

(a) $\nu = 3.23$ (b) $\nu = 6.02$ (c) $\nu = 8.81$

Figure 18. Incremental Unsteady Gust Loads vs Time for $L_g = 104.m$
$\theta_0 = -25.°$; $K_\theta = 3.217E05\, Nm/rad$; $\gamma = 0.866$; $\hat{r} = 1.15$
(- - - -: gust loads; ·····: aerodynamic loads due to the wing-tip deflection; — · —: inertial loads;
——: global loads)

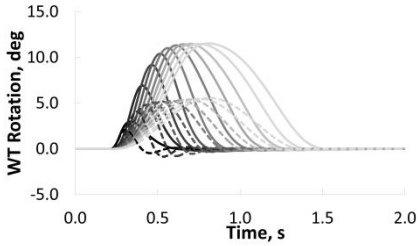

Figure 19. Linear vs Nonlinear Gust Response
$\theta_0 = -25.°$; $K_\theta = 3.217E05\, Nm/rad$; $\gamma = 0.866$; $\hat{r} = 1.15$; $\nu = 6.02$
(- - - -: linear model; ——: nonlinear model)

Figure 20 shows the loads envelope for different gust lengths and the overall moment and stiffness for the [$\theta_0 = -25.°$; $K_\theta = 3.217E05\, Nm/rad$; $\gamma = 0.5$; $\hat{r} = 1.98$] configuration for different values of the spring stiffness ratio ν. The comments related to the previous case remained valid also for this configuration, only a slight worsening on the loads alleviation performance was noticed. This effect was due to the higher adimensional radius $\hat{r}$ employed which caused the oblique springs to provide a negative stiffness contribution over a smaller range of rotation angles θ.

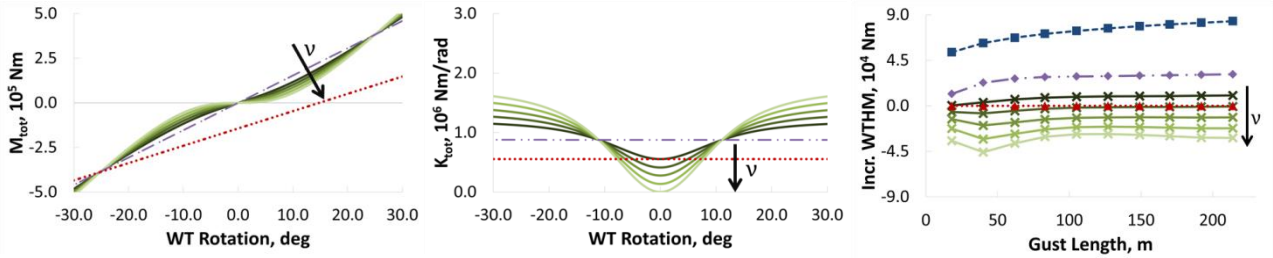

(a) $M_{tot}(\theta)$ (b) $K_{tot}(\theta)$ (c) Loads Envelope vs Gust Lengths

Figure 20. Nonlinear Gust Response
$\theta_0 = -25.°$; $K_\theta = 3.217E05\, Nm/rad$; $\gamma = 0.5$; $\hat{r} = 1.98$; $\nu = [0.5, 0.72, 0.93, 1.15, 1.36]$
(- - - -: fixed hinge model; — · · : linear model $K_\theta = 3.217E05\, Nm/rad$;
·····: linear model $K_\theta = 0.\, Nm/rad$; ——: nonlinear model)

Figures 21 and 22 show the loads envelope for different gust lengths and the overall moment and stiffness when $[\theta_0 = -12.5.°;\ K_\theta = 6.434E05\, Nm/rad;\ \gamma = 0.5;\ \hat{r} = 3.96]$ and $[\theta_0 = -12.5.°;\ K_\theta = 6.434E05\, Nm/rad;\ \gamma = 0.866;\ \hat{r} = 2.92]$ configurations were employed for different values of the spring stiffness ratio ν. For both the cases it was noticed how the loads of the nonlinear models were lower than those of the linear model with $[\theta_0 = -12.5.°;\ K_\theta = 6.434E05\, Nm/rad]$. Even though the designs with the higher stiffness ratios ν allowed very low stiffness values around the equilibrium point, the hinge moment envelopes exhibit loads that were always positive and higher than the ones of the linear model with $K_\theta \approx 0.\, Nm/rad$.

Again, this worsening in the alleviation performance can be attributed to the higher $\hat{r}$ employed. Equations (11) and (12) show that the lower are the initial wing-tip deflection θ_0 and the initial oblique springs inclination ($\gamma \to 1.$) the lower the resulting linear spring stiffness K_θ and pulley radius $\hat{r}$. The latter term is a fundamental parameter for the definition of the nonlinear contribution of the oblique springs; the lower that $\hat{r}$ is, the higher the wing-tip rotation needed to produce a given oblique spring's horizontal displacement. Therefore, the nonlinear effects will be spread over a longer range of folding angles leading to a smoother reduction of the aeroelastic stiffness. Once the geometry of the hinge device is fixed, the spring stiffness ratio ν can be used as a tuning parameter to control the reduction of the aeroelastic stiffness around the equilibrium point. The red dotted lines in Figs. 17(b) and 20-22(b), represent the aeroelastic stiffness of the linear hinge device with $K_\theta = 0.\, Nm/rad$, therefore they are purely characterized by the aerodynamic stiffness contribution and constitute the zero structural stiffness threshold. When $\nu > \nu_{qzss}$ the system presented a negative structural stiffness, which means K_{tot} is below the zero structural stiffness threshold, over the range of folding angles $\Delta\theta_{nss}$. Within $\Delta\theta_{nss}$ the structural hinge device generated a moment that can be exploited to allow faster and higher wing-tip rotation with respect to the linear model. The value of $\Delta\theta_{nss}$ is mainly a function of $\hat{r}$ and ν; the lower that $\hat{r}$ and the higher that ν are, the higher $\Delta\theta_{nss}$ as it can be seen by comparing Fig. 17(b) and Fig. 21(b), characterized respectively by $\hat{r} = 1.15$ and $\hat{r} = 3.96$.

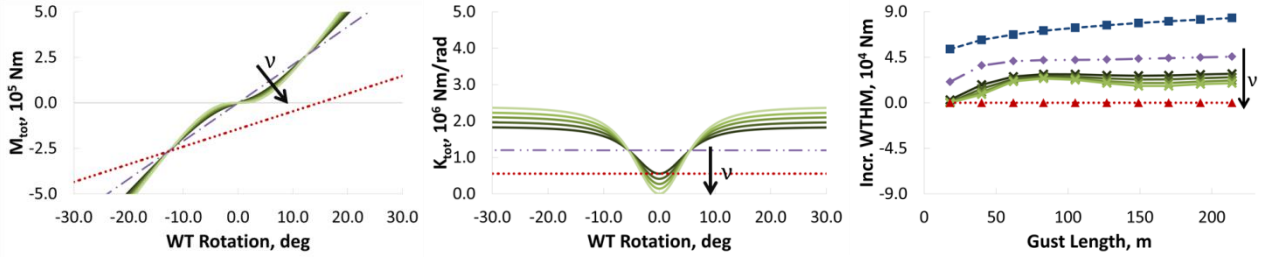

(a) $M_{tot}(\theta)$ (b) $K_{tot}(\theta)$ (c) Loads Envelope vs Gust Lengths

Figure 21. Nonlinear Gust Response
$\theta_0 = -12.5°$; $K_\theta = 6.434E05\, Nm/rad$; $\gamma = 0.5$; $\hat{r} = 3.96$; $\nu = [0.5, 0.61, 0.72, 0.82, 0.93]$
(- - - -: fixed hinge model; — · · : linear model $K_\theta = 6.434E05\, Nm/rad$;
·····: linear model $K_\theta = 0.\, Nm/rad$; ——: nonlinear model)

The effect of the non-dimensional radius $\hat{r}$ is highlighted in Fig. 23 that shows the time histories of the loads of the $[\theta_0 = -12.5.°;\ K_\theta = 6.434E05\, Nm/rad;\ \gamma = 0.866;\ \hat{r} = 2.92]$ design, for given gust length $L_g = 104.\, m$,

and for different values of ν. When the wing-tip was hit by the gust, the low aeroelastic stiffness value allowed the fast rotation of the device because of the small local stiffness. The high values of $\hat{r}$ led the structural stiffness to have a sudden increment after a small deflection of the device and the wing-tip was so not slowed down by the negative aerodynamic forces, but by the hinge structural stiffness increment. The results was a sudden stop of the folding device and so the generation of a positive peak of the inertial loads that, combined with the gust moments, overcame the negative contribution due to the wing-tip rotation. Such behavior was more pronounced for higher values of ν.

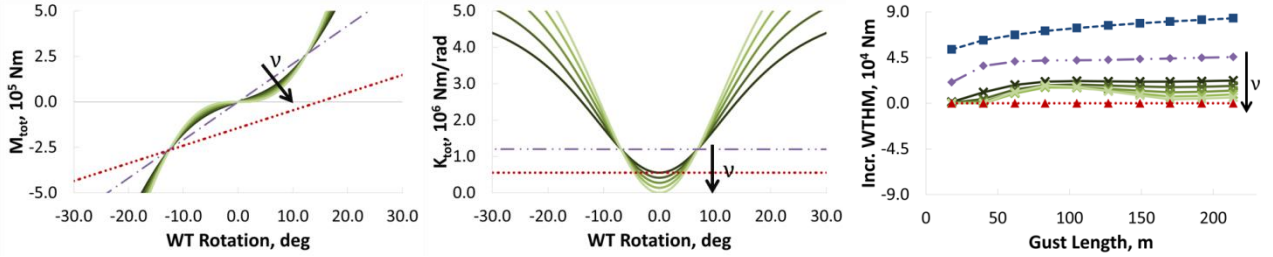

(a) $M_{tot}(\theta)$ (b) $K_{tot}(\theta)$ (c) Loads Envelope vs Gust Lengths

Figure 22. Nonlinear Gust Response
$\theta_0 = -12.5°$; $K_\theta = 6.434E05\ Nm/rad$; $\gamma = 0.866$; $\hat{r} = 2.92$; $\nu = [3.23, 3.93, 4.63, 5.32, 6.02]$
(- - - -: fixed hinge model; — · · : linear model $K_\theta = 6.434E05\ Nm/rad$;
·····: linear model $K_\theta = 0.\ Nm/rad$; ——: nonlinear model)

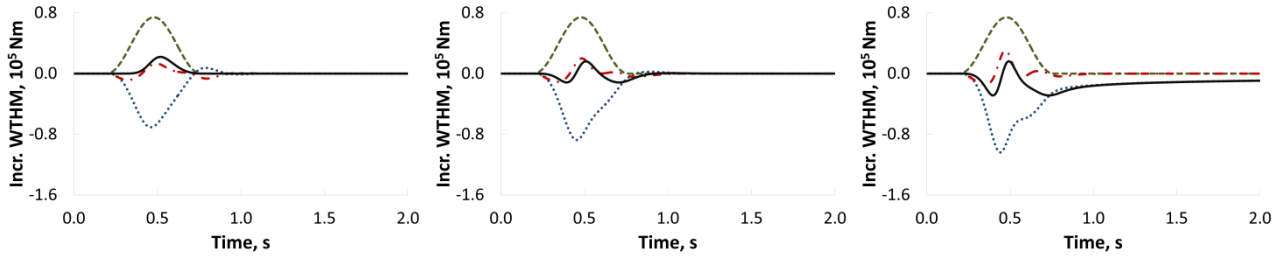

(a) $\nu = 3.23$ (b) $\nu = 4.63$ (c) $\nu = 6.02$

Figure 23. Incremental Unsteady Gust Loads vs Time for $L_g = 104.m$
$\theta_0 = -12.5°$; $K_\theta = 6.434E05\ Nm/rad$; $\gamma = 0.866$; $\hat{r} = 2.92$
(- - - -: gust loads; ·····: aerodynamic loads due to the wing-tip deflection; — · —: inertial loads;
——: global loads)

IV. Full Aircraft Model

An investigation of high static low dynamic aeroelastic stiffness hinge device applied on a full aircraft model is now presented. The purpose is an understanding of the dynamic response of the proposed device when the dynamic coupling of the wing-tip and main airframe is considered and how this affects the design of the hinge spring.

A. Structural Modeling

The commercial multibody code LMS Virtual.Lab Motion (VLM) was used for the aeroelastic analyses of the full aircraft model[15]. The software enables nonlinear dynamic simulations of rigid and flexible multibody systems. Many formulations have been proposed in the literature to include the flexibility of a subcomponent in a multibody analysis[16], such as the floating frame of reference technique, the finite segment method, the finite element incremental method etc. The floating frame of reference (FFR), is the formulation which has found the most widespread application and implementation in the commercial multibody packages, such as Virtual.Lab Motion. The FFR formulation infers that the configuration of a generic deformable body in the multibody system is identified by

using two sets of coordinates: the reference coordinates which define the location R and orientation Ψ of a generic body reference, and the elastic coordinates q_f which describe the body local deformations with respect to the body reference by using linear dynamic condensation techniques such as Rayleigh-Ritz methods. Therefore, despite the multibody code allows the modelling of nonlinear finite translations and rotations for the body reference coordinates, the elastic coordinates, with the related modal shapes, can only describe small and linear deformations. The selected modal shapes have to satisfy the kinematic constraints imposed on the boundaries of the related deformable body due to the connection chain between the different subcomponents; therefore Craig-Bampton[17] mode sets are generally defined to take attachment effects into account.

Aeroelastic simulations within the multibody package can be enabled through the definition of a user defined force element (UDF) to introduce linear unsteady aerodynamic forces into the system. However, a current limitation that arises is that it is possible to apply the aerodynamic forces to only one body of the multibody chain. The reason is that the UDF has been formerly developed for the simulation of landing manoeuvers with the inclusion of aeroelastic and gusts loads, which required the application of the aerodynamic forces only on the aircraft, but not on the landing gears. Therefore, for this work, it was not possible to consider the main airframe and the two wing-tips as three separate entities, since all of them experience aerodynamic forces. Thus, only a single body was defined to model the entire assembly.

With such a modeling approach, the wing-tips deflection was enabled through the use of a specific set of modal shapes used to describe the flexibility of the overall assembly. The idea was to use the set of flexible modes obtained when a very low hinge spring stiffness was defined; a zero stiffness value was avoided to prevent numerical singularities during the modal analysis. This approach was implemented by setting the first two flexible modes as local symmetric and anti-symmetric pseudo-rigid wing-tips deflection as shown in Fig. 24(a, b). Such modal shapes are by definition orthogonal with the remaining flexible modes that involve a combination of wing-tips and main airframe deformations, Fig. 24(c, d), therefore they could be used to describe independent wing-tip rotations. It is important to point out that the wing-tip deflections were therefore modelled as linear local deformations and not as finite nonlinear rotations. The overall span reduction due to the wing-tips deflection was not considered.

Linear and nonlinear hinge devices, such as springs, dampers or actuators, can be modeled by applying external moments on the hinge nodes along the hinge axis in order to simulate the related restoring moments on the wing-tips and main airframe, as shown in Fig. 25. The hinge moments could be defined as linear or nonlinear functions of the wing-tip folding angle and, once projected onto the structural modes, defined as a set of generalized forces that could excite mainly the local wing-tip modes and so drive the wing-tips motion. The UDF capability was employed also to model the local hinge moments applied on the model. In this way it was possible to model local structural nonlinearities still using a linear set of normal modes to describe the dynamic response of the structure.

The numerical structural model used for these investigations, involved a $100\,Kg$ wing-tip model with a $25°$ hinge angle and a hinge spring stiffness of $1.E0\ Nm/rad$. Since a free flight condition was considered and no attachments effects between the airframe and the wing-tips were needed to be taken into account, a set of normal modes with free-free boundary conditions was so used to model the flexible airframe. A total of 44 flexible modes, up to $25.\,Hz$, were considered, with residual vectors also added to reduce the error due to modal truncation.

B. Aerodynamic Modeling

The DLM was employed once again to model the aerodynamic forces of the full aircraft model. As the multibody software characterized by a time solver, Roger's rational fraction approximation method was again employed leading to the formulation for the aerodynamic forces such that

$$F_{Aero} = q_{dyn}\left\{\left[Q_0\xi + \frac{c}{2V}Q_1\dot{\xi} + \left(\frac{c}{2V}\right)^2 Q_2\ddot{\xi}\right] + \left[Q_{x0}\delta + \frac{c}{2V}Q_{x1}\dot{\delta} + \left(\frac{c}{2V}\right)^2 Q_{x2}\ddot{\delta}\right]\right. \tag{23}$$

$$\left. + \left[Q_{g0}w + \frac{c}{2V}Q_{g1}\dot{w} + \left(\frac{c}{2V}\right)^2 Q_{g2}\ddot{w}\right] + \sum_{l=1}^{N_{Poles}} R_l\right\}$$

$$\dot{R}_l = -b_l \frac{2V}{c} IR_l + Q_{2+l}\dot{\xi} + Q_{x2+l}\dot{\delta} + Q_{g2+l}\dot{w} \qquad l = 1, \dots, N_{Poles} \tag{24}$$

where $Q_{(N_{Modes}+6\ X\ N_{Modes}+6)}$, $Q_{x(N_{Modes}+6\ X\ N_{ControlSurf})}$ and $Q_{g(N_{Modes}+6\ X\ N_{Panels})}$ are respectively the generalized aerodynamic forces matrices related to the generalized coordinates ξ, control surfaces vector δ and gust vector w, defined as in Eqs. (16) and (17). Given that no physical control surfaces were defined on structural model, as shown in Fig. 2(a), the aerodynamic forces due to the control surfaces deflection were evaluated by means of transpiration boundary conditions, i.e. by applying a local variation of the downwash velocity on the control surfaces' aerodynamic panels without actually rotating them.

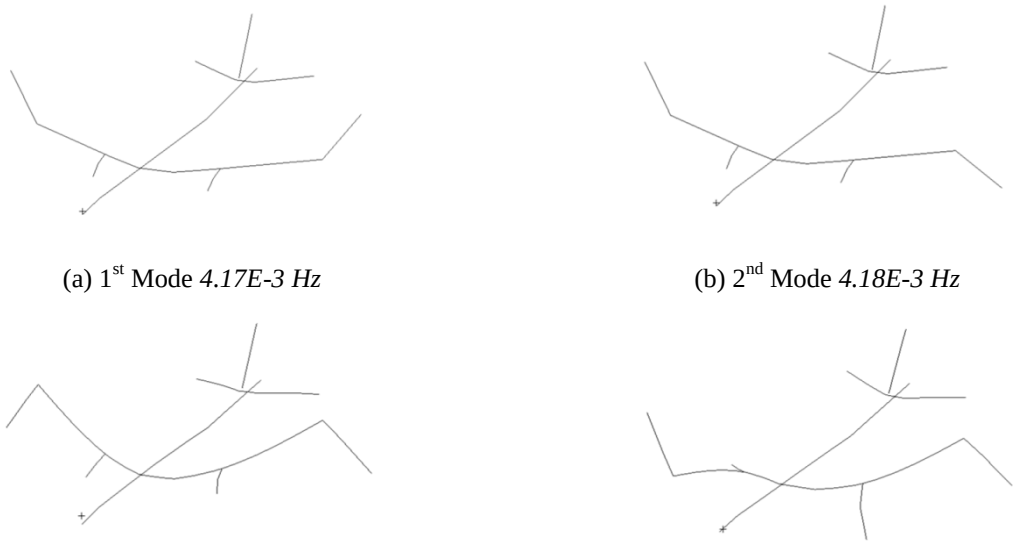

(a) 1st Mode *4.17E-3 Hz* (b) 2nd Mode *4.18E-3 Hz*

(c) 3rd Mode *2.22E0 Hz* (d) 4th Mode *2.54E0 Hz*

Figure 24. Lower Frequencies Structural Modes

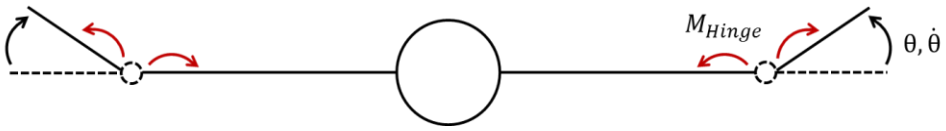

Figure 25. Applied Hinge Moments

C. Equation of Motion

The nonlinear dynamics equations of the system are described as

$$\bar{M}\ddot{\xi} + \bar{D}\dot{\xi} + \bar{K}\xi = \bar{Q}_v + \bar{Q}_e + \bar{F}_{Aero} + \bar{M}_{struct}$$

$$\begin{bmatrix} \bar{M}_{RR} & \bar{M}_{R\Psi} & \bar{M}_{Rf} \\ \bar{M}_{\Psi R} & \bar{M}_{\Psi\Psi} & \bar{M}_{\Psi f} \\ \bar{M}_{fr} & \bar{M}_{f\Psi} & \bar{M}_{ff} \end{bmatrix} \begin{Bmatrix} \ddot{R} \\ \ddot{\Psi} \\ \ddot{q}_f \end{Bmatrix} + \begin{bmatrix} 0 & 0 & 0 \\ 0 & 0 & 0 \\ 0 & 0 & \bar{D}_{ff} \end{bmatrix} \begin{Bmatrix} \dot{R} \\ \dot{\Psi} \\ \dot{q}_f \end{Bmatrix} + \begin{bmatrix} 0 & 0 & 0 \\ 0 & 0 & 0 \\ 0 & 0 & \bar{K}_{ff} \end{bmatrix} \begin{Bmatrix} R \\ \Psi \\ q_f \end{Bmatrix}$$

$$= \begin{Bmatrix} \bar{Q}_{v_R} \\ \bar{Q}_{v\Psi} \\ \bar{Q}_{v_f} \end{Bmatrix} + \begin{Bmatrix} \bar{Q}_{e_R} \\ \bar{Q}_{e\Psi} \\ \bar{Q}_{e_f} \end{Bmatrix} + \begin{Bmatrix} \bar{F}_{Aero_R} \\ \bar{F}_{Aero\Psi} \\ \bar{F}_{Aero_f} \end{Bmatrix} + \begin{Bmatrix} 0 \\ 0 \\ \bar{M}_{struct}(q_f)_f \end{Bmatrix} \tag{25}$$

where ξ is the vector of the generalized coordinates of the body which includes the rigid body translations $\{R_1, R_2, R_3\}$ and rotations $\{\Psi_1, \Psi_2, \Psi_3\}$ and the modal elastic coordinates $\{q_{f1}, \dots q_{fN_{Modes}}\}$ related to the linear flexible modes, as in Fig. 24, $\bar{M}, \bar{D}, \bar{K}$ are the generalized mass, damping and stiffness matrices, $\bar{Q}_v$ are the quadratic velocity forces (Coriolis and centrifugal terms), $\bar{Q}_e$ are the generalized external forces, due in this case only to gravity, $\bar{F}_{Aero}$ are the generalized aerodynamic forces and $\bar{M}_{struct}$ are the generalized moments due to the hinge device. The latter were evaluated by projecting onto the modal basis the hinge moment in Eq. (7).

For the full aircraft model the overall static aeroelastic hinge moment and stiffness in Eqs. (9) and (10) can be expressed as

$$M_{tot} = M_{struct} - K_{aero\theta}\theta - K_{aero\alpha}\alpha - K_{aero\delta_e}\delta_e - M_g \tag{26}$$

$$K_{tot} = K_{struct} - K_{aero\theta} \tag{27}$$

where $K_{aero\alpha}\alpha$ and $K_{aero\delta_e}\delta_e$ are the static aerodynamic hinge moments for a given angle of attack and elevator deflection and M_g represents the contribution of the gravity. Such external loads generated also a static deformation of the entire aircraft with a consequent variation of the aerodynamic forces distribution. The flexibility effects could not be neglected and have been taken into account considering the nonlinear variation of the different load contributions with the dynamic pressure as reported in Fig. 26. Despite the same wing-tip geometry was defined for the single degree of freedom and full aircraft models, the related aerodynamic stiffness differ because of the aerodynamic coupling effects of the wing-tip's and airframe's aerodynamic panels as well as for the wing twisting effects considered in the full aircraft model. The same observations also occurred for $q_{dyn}Q_{\alpha 0}$ and $K_{aero\alpha}$.

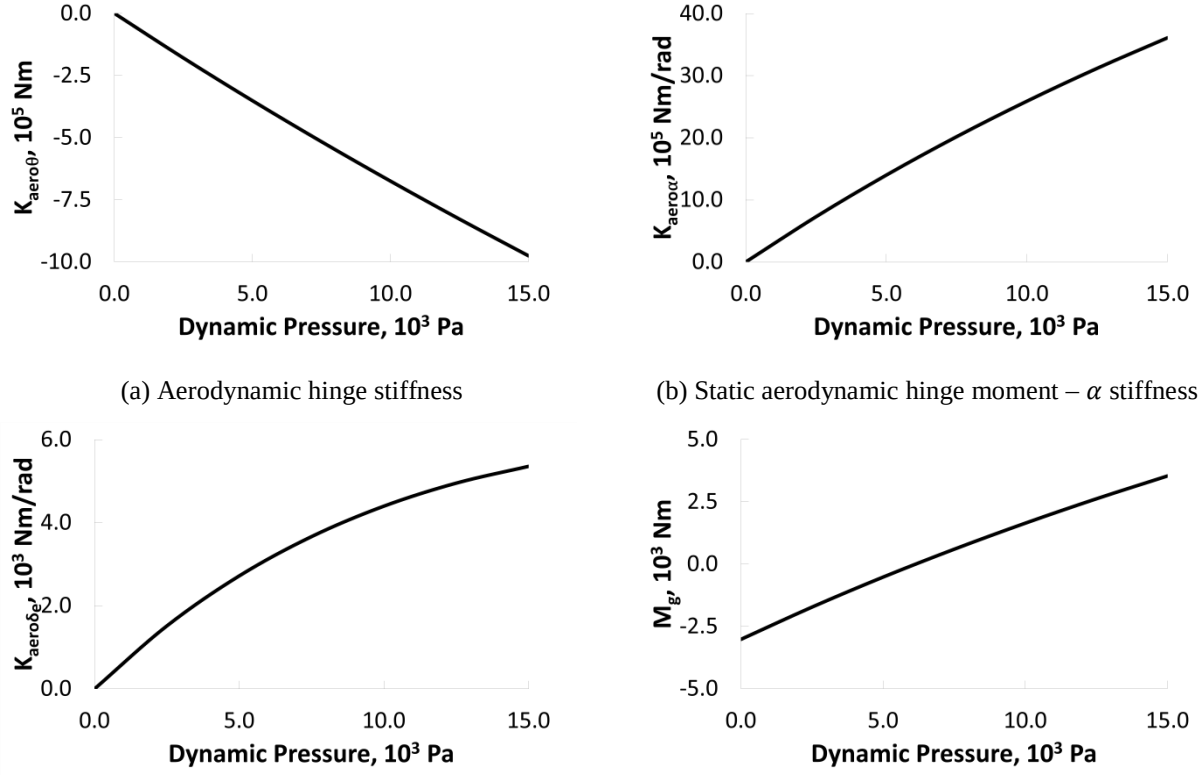

(a) Aerodynamic hinge stiffness

(b) Static aerodynamic hinge moment – α stiffness

(c) Static aerodynamic hinge moment – δ_e stiffness

(d) Gravity hinge moment

Figure 26. Hinge Aeroelastic Static Moments Contribution

D. Results

Also for the full aircraft model it was not possible to separate the static and the dynamic response due to the nonlinearity of the hinge device, therefore the dynamic gust response analyses were performed starting from a trimmed flight configuration. The same flight condition, in terms of Mach value, altitude and dynamic pressure, and the same "*1-cosine*" gusts family considered for the single degree of freedom model were defined for the full aircraft model as well.

Several structural configurations were considered by varying the hinge device design parameters according the high static low dynamic aeroelastic stiffness concept introduced in the previous section. All the investigated hinge device designs that satisfied the condition $\theta_{trim} = 0°$ led to the same trim flight condition given by an angle of attack of $6.25°$ and elevator deflection of $-12.39°$. Figure 27 shows an example of the different structural configuration between the initial and the trimmed flight condition.

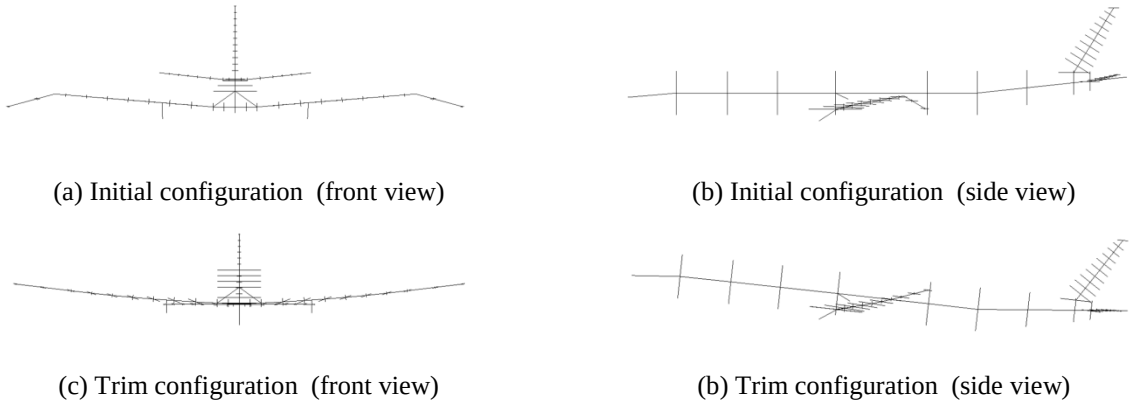

(a) Initial configuration (front view)

(b) Initial configuration (side view)

(c) Trim configuration (front view)

(b) Trim configuration (side view)

Figure 27. Static Trim Deformation

Several spring designs were considered for the nonlinear gust response analyses: four different wing-tip initial folding angles, with the related linear spring stiffness, defined in Eq. (11), were selected $[\theta_0 = -12.5.°;\ K_\theta = 1.237E06\ Nm/rad]$, $[\theta_0 = -25.°;\ K_\theta = 6.186E05\ Nm/rad]$, $[\theta_0 = -37.5°;\ K_\theta = 4.124E05\ Nm/rad]$ and $[\theta_0 = -50.°;\ K_\theta = 3.093E05\ Nm/rad]$. For each of these combinations, two sets of oblique springs with an inclination of $\sigma = 30.°$ (i.e. $\gamma = 0.866$) and $\sigma = 60.°$ (i.e. $\gamma = 0.5$) were specified; the related non-dimensional pulley radii $\hat{r}$ were defined according Eq. (12). Finally, ν was varied for each structural configuration between the related ν_{qzss} and ν_{qzas} values.

Figures 27-34(a) show the aeroelastic stiffness curves as a function of the wing-tip folding angle for the different structural designs. As for the single degree of freedom model, the lower that $\hat{r}$ was, the higher the range of rotations $\Delta\theta_{nss}$ over which the structural hinge device generated a moment so that the folding angle can be exploited to allow faster and higher wing-tip rotation and so enhance the loads alleviation performance with respect to the linear model.

Figures 27-34(b) show the incremental gust loads envelope for different gust lengths for the different structural designs. All the investigated designs allowed a reduction of the maximum loads with respect to the fixed hinge model; for the design in Figs. 27(b) and 28(b) the loads were always higher than the ones of the baseline model and presented only slight reduction for increasing values of ν; for all the remaining designs the maximum loads were always equal or lower than the ones of the baseline model and higher values of ν allowed better alleviation performance.

The reported results highlight again how the loads alleviation capabilities are not only function of the value of the aeroelastic stiffness at the static equilibrium point, but also of the range of rotation $\Delta\theta_{nss}$ over which the structural stiffness is kept negative. When the gust hits the aircraft, all the investigated hinge designs allowed a fast wing-tip rotation given the low aeroelastic stiffness K_{tot} at $\theta_{trim} = 0.°$. When high values of $\hat{r}$ were defined, as in Figs. 27 and 28, the aeroelastic stiffness shows a sudden increment after a small deflection of the device. As a result, the system experienced lower wing-tip deflections, and therefore could generate a lower negative lift contribution to counteract the positive gust loads, furthermore the sudden braking of the device generated also a positive peak of the inertial loads which reduced the loads alleviation capabilities. Lower values of $\hat{r}$, as in Figs. 29-34, allowed the system not suffer of such limitation of the loads alleviation capabilities.

Regarding the minimum loads, they were always larger than those of the baseline model and in some case even higher than those of the fixed hinge model. Nevertheless structural sizing and loads assessment require the combination of the positive static trim loads with those from the incremental gust, as a consequence the positive gust loads, which were reduced by the wing-tip device, are the most critical for the structure.

A better understanding of the system response can be found looking at the time histories of the wing-tip deflections and incremental wing root bending moments, reported in Figs. 28(c, d), 30(c, d), 32(c, d) and 34(c, d), for the different structural configurations and a gust length of $214\ m$, which was the one that generated the highest hinge moments and wing-tip deflections. To allow a more direct comparison of the deflections induced by the gusts for the different models, Figs 28-34(c) report the actual wing-tip deflections for the nonlinear models (solid lines), and only the incremental rotations for the linear model with $K_\theta = 0. Nm/rad$ (dotted lines), being for such configuration $\theta_{trim} = 26.96°$. It can be seen that high ν and low $\hat{r}$ minimize K_{tot} and maximize $\Delta\theta_{nss}$ leading to good loads alleviation performance via higher and faster rotations. The structural configuration reported in Figs. 27 and 28 were characterized by very high $\hat{r}$, respectively 3.70 and 2.29, and low $\Delta\theta_{nss}$; the sudden increment of the aeroelastic stiffness allowed wing-tip rotations lower than the incremental deflections of the linear model, as in Fig. 28(c), therefore the wing root bending moments were lower than those of the fixed hinge model, but higher than the baseline model. The same problem was observed for the configurations in Figs. 29 and 30, but only for the longer gust lengths, $L_g \geq 170\ m$, that produced higher wing-tip deflections for which $\Delta\theta_{nss}$ was not enough to allow an optimal loads alleviation. All the other investigated structural designs experienced wing-tip deflections equal or higher than those of the linear model with $K_\theta = 0. Nm/rad$ and maximum wing root bending moments equal or lower than the baseline model. High values of ν allowed higher wing-tip deflections and therefore lower loads. The highest wing-tip deflection was experienced by the structural design reported in Fig. 34, with $\hat{r} = 0.57$, for which $\theta_{max} \approx 27.°$, with respect the 11.93° of maximum wing-tip incremental deflection of the linear model; from Eq. (1) this response means a variation of the local wing-tip angle of attack of $\Delta\alpha_{wt} = -12.15°$ and so an actual angle of attack of $\alpha_{wt} = -5.90°$ considering the overall trim angle of attack $\alpha = 6.25°$.

When a linear spring with negligible stiffness was employed, the aircraft did not experience any loads increment due to a positive "1-cosine" gust, the wing-tip motion was driven only by the gust loads which allowed the generation of a negative lift contribution that balanced that due to a positive gust leading the wing-tip to be mostly unloaded[1] and so the extended wing-tip model to have incremental gust loads close to the baseline model. The negative stiffness contribution due to the nonlinear oblique springs allowed higher wing-tip deflections resulting in the generation of a negative lift that overcame the gust loads, leading the wing-tip to generate overall negative incremental loads and so leading the aircraft to experience incremental gust loads lower than those of the baseline model.

For $\nu \approx \nu_{qzss}$ the analyzed nonlinear models were characterized by an aeroelastic stiffness close to that of the linear model with $K_\theta = 0. Nm/rad$ in the neighborhood of the equilibrium position $\theta_{trim} = 0.°$, which led to very similar, if not equal, trend of the incremental wing root bending moment and wing-tip gust responses.

For all the investigated designs high values of ν enabled a low aeroelastic stiffness leading to a reduction of the positive gust loads because of the fast upward wing-tip rotation. The drawback was given by the fact that, because of the low aeroelastic stiffness, the wing-tip needed more time to recover the original undeflected configuration, as showed in Figs. 27-34(c). Such slower wing-tip dynamics, following the initial gust positive peak, led to a delay of the wing-tip response with respect the wing root bending moment which is the main reason behind the worsening of the loads alleviation capabilities for negative gust loads[1]. Moreover for all the investigated designs when $\nu \approx \nu_{qzas}$ the wing-tips were not able to recover the original undeflected configuration after the gust. The aeroelastic stiffness of the system was too small to balance the variation of the static loads acting on the hinge due to the variation of the angle of attack after the gust. Such an effect could not be captured by the single degree of freedom model since the angle of attack was considered as a constant value during the simulation, and no rigid pitch or heave motion of the wing-tip device were taken into account.

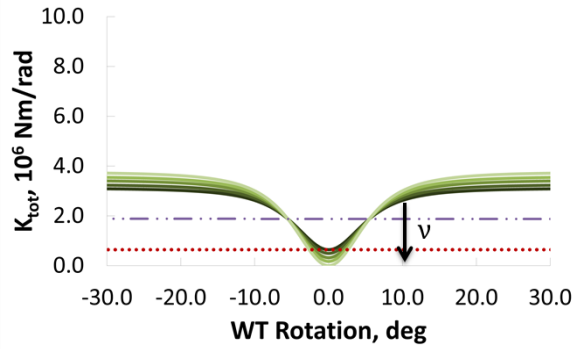

(a) $K_{tot}(\theta)$

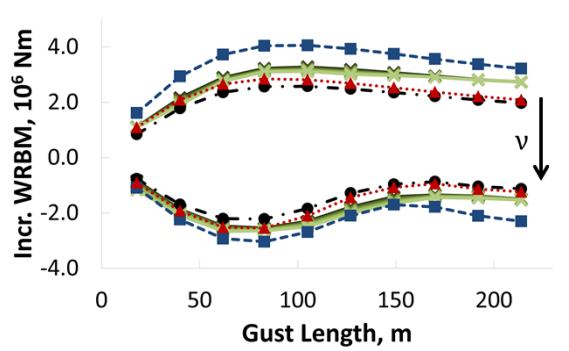

(b) Loads Envelope vs Gust Lengths

Figure 27. Nonlinear Gust Response
$\theta_0 = -12.5°$; $K_\theta = 1.237E06\ Nm/rad$; $\gamma = 0.5$; $\hat{r} = 3.70$; $\nu = [0.5, 0.56, 0.63, 0.69, 0.76]$
(– – –: fixed hinge model; — · · : linear model $K_\theta = 1.237E06\ Nm/rad$;
·····: linear model $K_\theta = 0.\ Nm/rad$; — · —: baseline model; ——: nonlinear model)

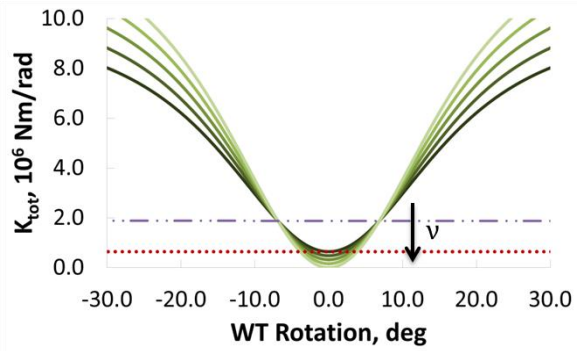

(a) $K_{tot}(\theta)$

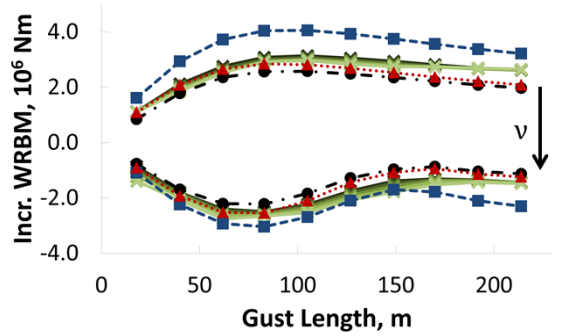

(b) Loads Envelope vs Gust Lengths

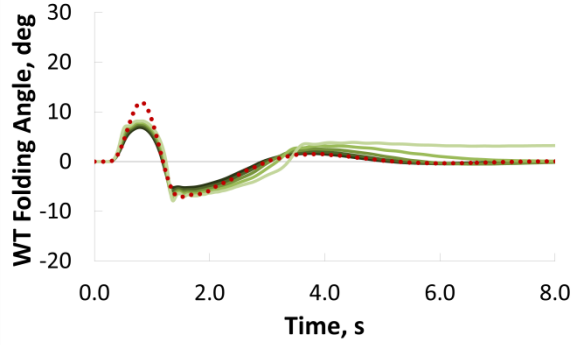

(c) Wing-tip folding angle - time histories for *Lg=214 m*

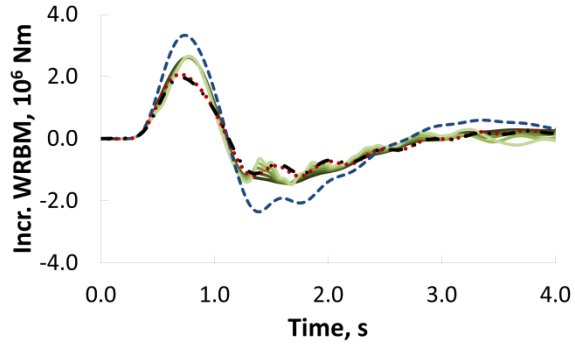

(d) Incremental WRBM - time histories for *Lg=214 m*

Figure 28. Nonlinear Gust Response
$\theta_0 = -12.5°$; $K_\theta = 1.237E06\ Nm/rad$; $\gamma = 0.866$; $\hat{r} = 2.29$; $\nu = [3.23, 3.65, 4.07, 4.49, 4.91]$
(– – –: fixed hinge model; — · · : linear model $K_\theta = 1.237E06\ Nm/rad$;
·····: linear model $K_\theta = 0.\ Nm/rad$; — · —: baseline model; ——: nonlinear model)

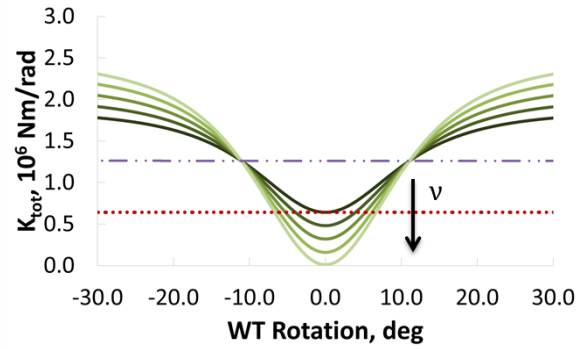

(a) $K_{tot}(\theta)$

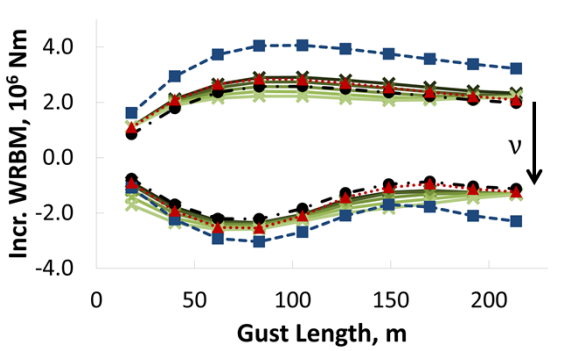

(b) Loads Envelope vs Gust Lengths

Figure 29. Nonlinear Gust Response
$\theta_0 = -25.°$; $K_\theta = 6.186E05\ Nm/rad$; $\gamma = 0.5$; $\hat{r} = 1.98$; $\nu = [0.5, 0.73, 0.96, 0.89, 1.01]$
(- - - -: fixed hinge model; — · · : linear model $K_\theta = 6.186E05\ Nm/rad$;
·····: linear model $K_\theta = 0.\ Nm/rad$; — · —: baseline model; ——: nonlinear model)

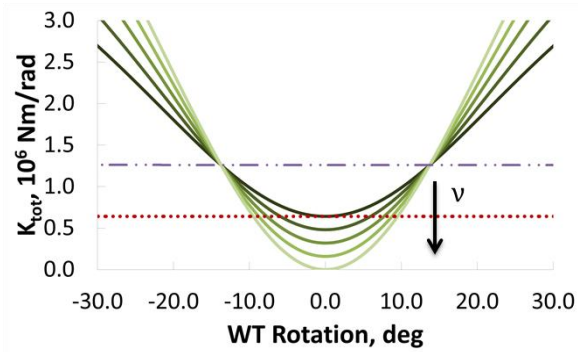

(a) $K_{tot}(\theta)$

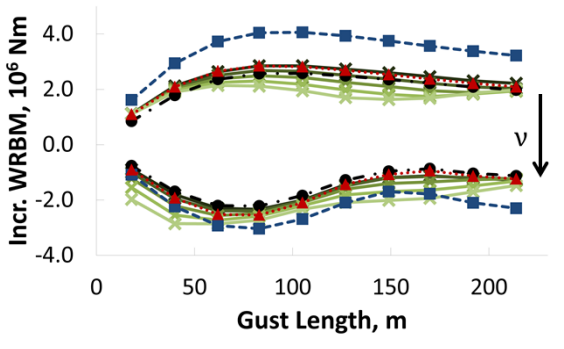

(b) Loads Envelope vs Gust Lengths

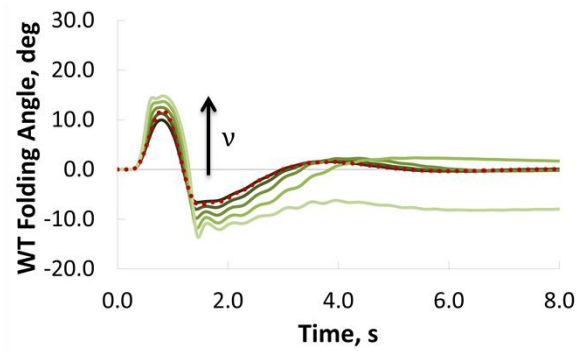

(c) Wing-tip folding angle - time histories for *Lg=214 m*

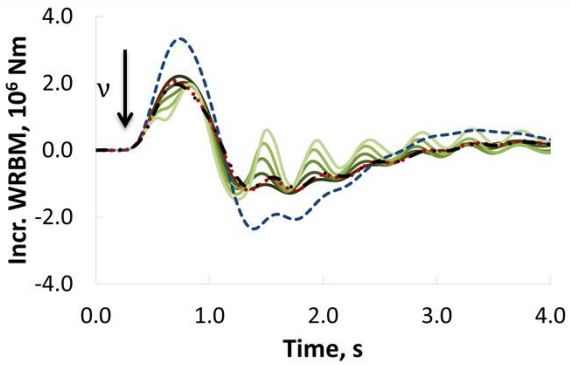

(d) Incremental WRBM - time histories for *Lg=214 m*

Figure 30. Nonlinear Gust Response
$\theta_0 = -25.°$; $K_\theta = 6.186E05\ Nm/rad$; $\gamma = 0.866$; $\hat{r} = 1.15$; $\nu = [0.5, 0.73, 0.96, 0.89, 1.01]$
(- - - -: fixed hinge model; — · · : linear model $K_\theta = 6.186E05\ Nm/rad$;
·····: linear model $K_\theta = 0.\ Nm/rad$; — · —: baseline model; ——: nonlinear model)

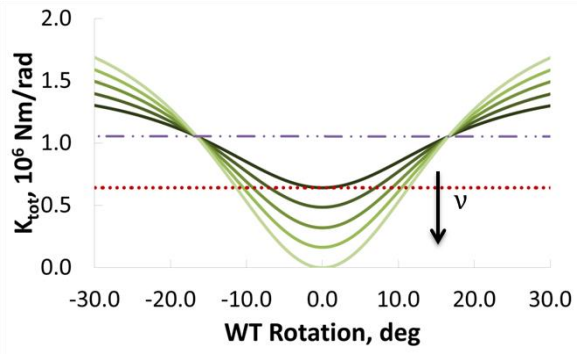

(a) $K_{tot}(\theta)$

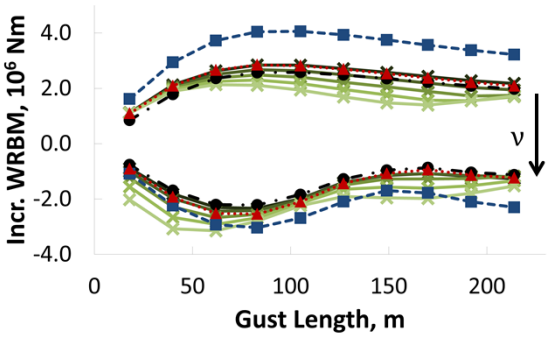

(b) Loads Envelope vs Gust Lengths

Figure 31. Nonlinear Gust Response
$\theta_0 = -37.5°$; $K_\theta = 4.124E05\ Nm/rad$; $\gamma = 0.5$; $\hat{r} = 1.32$; $\nu = [0.5, 0.69, 0.89, 1.08, 1.28]$
(– – –: fixed hinge model; — · · : linear model $K_\theta = 4.124E05\ Nm/rad$;
·····: linear model $K_\theta = 0.\ Nm/rad$; — · —: baseline model; ——: nonlinear model)

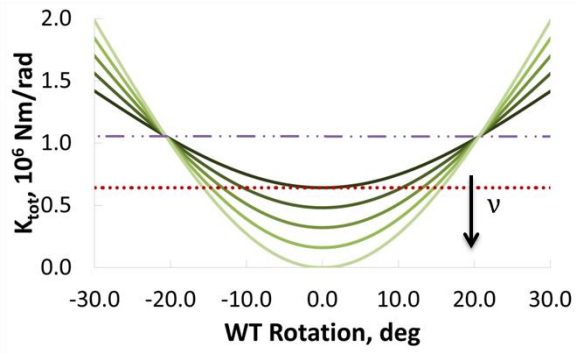

(a) $K_{tot}(\theta)$

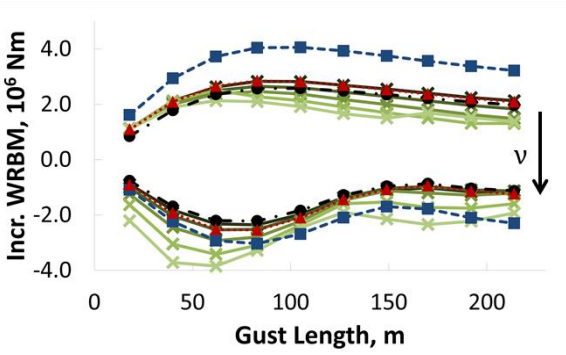

(b) Loads Envelope vs Gust Lengths

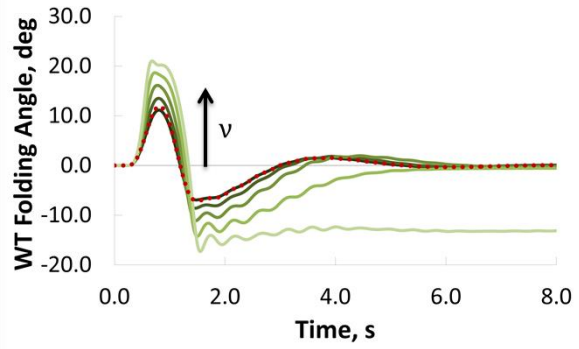

(c) Wing-tip folding angle - time histories for *Lg=214 m*

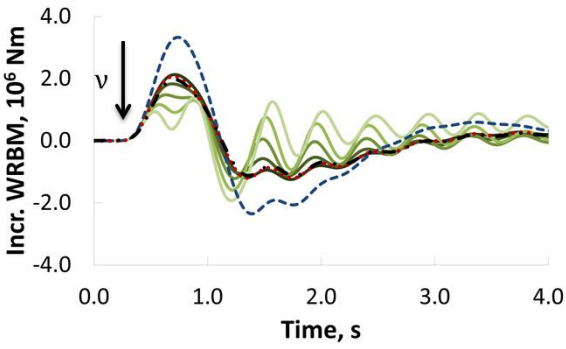

(d) Incremental WRBM - time histories for *Lg=214 m*

Figure 32. Nonlinear Gust Response
$\theta_0 = -37.5°$; $K_\theta = 4.124E05\ Nm/rad$; $\gamma = 0.866$; $\hat{r} = 0.76$; $\nu = [3.23, 4.49, 5.74, 7, 8.26]$
(– – –: fixed hinge model; — · · : linear model $K_\theta = 4.124E05\ Nm/rad$;
·····: linear model $K_\theta = 0.\ Nm/rad$; — · —: baseline model; ——: nonlinear model)

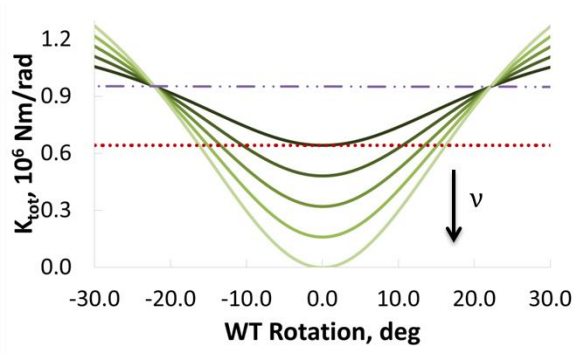

(a) $K_{tot}(\theta)$

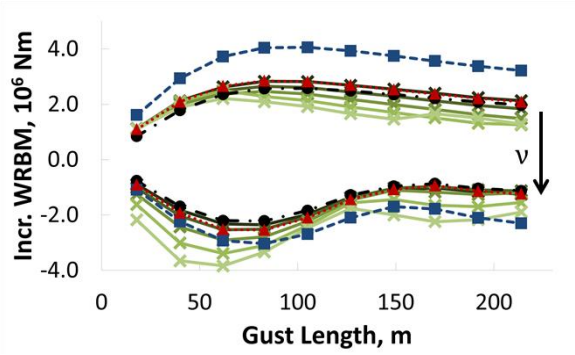

(b) Loads Envelope vs Gust Lengths

Figure 33. Nonlinear Gust Response
$\theta_0 = -50.°$; $K_\theta = 3.093E05\ Nm/rad$; $\gamma = 0.5$; $\hat{r} = 0.99$; $\nu = [0.5, 0.76, 1.02, 1.28, 1.54]$
(– – –: fixed hinge model; — · · : linear model $K_\theta = 3.093E05\ Nm/rad$;
·····: linear model $K_\theta = 0.Nm/rad$; — · —: baseline model; ——: nonlinear model)

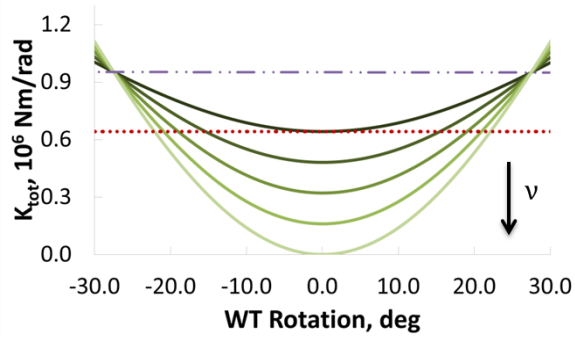

(a) $K_{tot}(\theta)$

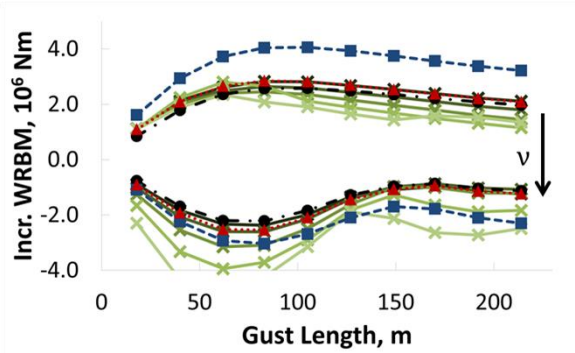

(b) Loads Envelope vs Gust Lengths

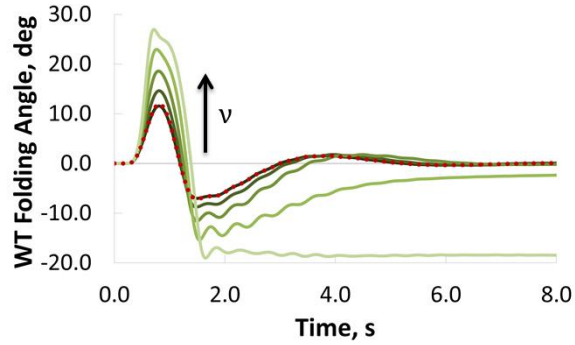

(c) Wing-tip folding angle - time histories for *Lg=214 m*

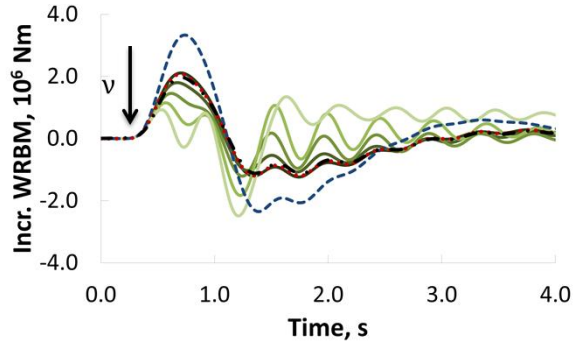

(d) Incremental WRBM - time histories for *Lg=214 m*

Figure 34. Nonlinear Gust Response
$\theta_0 = -50.°$; $K_\theta = 3.093E05\ Nm/rad$; $\gamma = 0.866$; $\hat{r} = 0.57$; $\nu = [3.23, 4.91, 6.58, 8.26, 9.93]$
(– – –: fixed hinge model; — · · : linear model $K_\theta = 3.093E05\ Nm/rad$;
·····: linear model $K_\theta = 0.Nm/rad$; — · —: baseline model; ——: nonlinear model)

V. Conclusions

A preliminary investigation into the use of nonlinear folding wing-tips as a gust loads alleviation device was performed using a single degree of freedom wing-tip model and a representative civil jet aircraft aeroelastic model. A wing-tip device was connected to the wings with a hinge and the effect of a nonlinear hinge device on the response to "1-cosine" gusts was investigated. All results were related to the loads acting on a baseline model which consisted of the aircraft without wing-tips, i.e. 20% less span.

A high static low dynamic aeroelastic stiffness mechanism was designed to allow a device stiff enough to keep the wing-tip undeflected during the cruise, while allowing fast and significant deflections in the case of a vertical gust with consequent reduction of the incremental loads.

The use of a nonlinear spring device enabled an improvement in loads alleviation capabilities compared to the linear device, reducing the incremental wing root bending moments to smaller levels compared to those of the baseline model. It was proven that significant loads alleviation were possible when the system exhibited a low overall stiffness around the trim equilibrium point for a large enough range of deflection angles. The negative stiffness contribution of the oblique springs allowed higher and faster wing-tip deflections resulting in a reduction of the gust effect. Moreover, the passive hinge device designs allowed the folding device to recover the original undeflected configuration after the gust.

Through proper design of the wing-tip device it will be possible to increase the wing aspect ratio with little, if any, increase or even a reduction of the gust loads experienced by the aircraft, leading to better aerodynamic efficiency and/or reduced structural weight on existing platforms.

VI. Acknowledgements

The research leading to these results has received funding from the European Community's Marie Curie Initial Training Network (ITN) on Aircraft Loads Prediction using Enhanced Simulation (ALPES) FP7-PEOPLE-ITN-GA-2013-607911 and also the Royal Academy of Engineering. The partners in the ALPES ITN are the University of Bristol, Siemens PLM Software and Airbus Operations Ltd.

References

[1]Castrichini A.,Hodigere Siddaramaiah. V., Calderon. D.E., Cooper J.E., Wilson T. & Lemmens Y., "Preliminary Investigation of Use of Flexible Folding Wing-Tips for Static and Dynamic Loads Alleviation" 4th RAeS Aircraft Structural Design Conference. Belfast, October 2014.

[2]Khodaparast H.H, Cooper J.E., "Rapid Prediction of Worst Case Gust Loads Following Structural Modification", AIAA Journal, Vol. 52, No. 2 (2014), pp. 242-254.

[3]Gatto A., Mattioni F. and Friswell M. I., "Experimental Investigation of Bistable Winglets to Enhance Aircraft Wing Lift Takeoff Capability", Journal of Aircraft, Vol. 46, No. 2 (2009), pp. 647-655.

[4]Arrieta A. F., Bilgen O., Friswell M. I., Hagedorn P., "Dynamic control for morphing of bi-stable composites", Journal of Intelligent Material Systems and Structures, 24(3) 266–273.

[5] Bilgen O.,Arrieta A. F., Friswell M. I., Hagedorn P., "Dynamic control of a bistable wing under aerodynamic loading", Smart Materials and Structures, 22 (2013) 025020.

[6]Carrella, A., Brennan M. J. & Waters T. P., "Static analysis of a passive vibration isolator with quasi-zero-stiffness characteristic." Journal of Sound and Vibration 301.3 (2007): 678-689.

[7]Rivin E.I., "Passive Vibration Isolation", ASME Press, New York, 2001.

[8]Alabuzhev P., Gritchin A., Kim L., Migirenko G., Chon V., Stepanov P., "Vibration Protecting and Measuring Systems with Quasi-Zero Stiffness", Hemisphere Publishing, New York, 1989.

[9]Platus D.L., "Negative-stiffness-mechanism vibration isolation systems", SPIE—Vibration Control in Microelectronics, Optics and Metrology 1619 (1991) 44–54.

[10]Schenk M & Guest S.D., "On zero stiffness", Proceedings of the Institution of Mechanical Engineers, Part C: Journal of Mechanical Engineering Science, 228. pp. 1701-1714. ISSN 0954-406.

[11]Albano E., Rodden W.P., "A Doublet-Lattice Method for Calculating Lift Distributions on Oscillating Surfaces in Subsonic Flows", AIAA Journal v7 n2 1969 pp 279-285.

[12]Rodden W.P., Johnson E.H. , "MSC/NASTRAN Aeroelastic Analysis' User's Guide", MSC Software, USA, 1994.

[13]Wright J.R., Cooper J.E., “Introduction to Aircraft Aeroelasticity and Loads”, John Wiley, 2007.

[14]Roger K.L., “Airplane Math Modeling Methods For Active Control Design”, AGARD Structures and Materials Panel, number CP-228, pp 4-11, 1977.

[15]Castrichini A.,Hodigere Siddaramaiah. V., Calderon. D.E., Cooper J.E., Wilson T. & Lemmens Y., “Nonlinear Folding Wing-Tips for Gust Loads Alleviation”, 56th AIAA/ASCE/AHS/ASC Structures, Structural Dynamics, and Materials Conference. January 2015.

[16]Shabana A., “Dynamics of Multibody Systems”, John Wiley Sons, New York, 1989.

[17]Bampton, M.C.C., Craig, R.R. Jr., "Coupling of substructures for dynamic analyses." AIAA Journal, Vol. 6, No. 7 (1968), pp. 1313-1319.